

Review

Luminescent Metal–Organic Framework Thin Films: From Preparation to Biomedical Sensing Applications

Zhengluan Liao ^{1,2}, Tifeng Xia ³, Enyan Yu ^{1,2,*} and Yuanjing Cui ^{3,*} 

¹ Department of Psychiatric, Zhejiang Provincial People's Hospital, Hangzhou 310014, China; liaozhengluan@163.com

² People's Hospital of Hangzhou Medical College, Hangzhou 310014, China

³ School of Materials Science and Engineering, Zhejiang University, Hangzhou 310027, China; 11426009@zju.edu.cn

* Correspondence: yuenyan@aliyun.com (E.Y.); cuiyj@zju.edu.cn (Y.C.); Tel.: +86-571-8589-3767 (E.Y.)

Received: 4 August 2018; Accepted: 17 August 2018; Published: 23 August 2018



Abstract: Metal-organic framework (MOF) thin films are receiving increasing attention in a number of different application fields, such as optoelectronics, gas separation, catalysis electronic devices, and biomedicine. In particular, their tunable composition and structure, accessible metal sites and potential for post-synthetic modification for molecular recognition make MOF thin films promising candidates for biosensing applications. Compared with solution-based powdery probes, film-based probes have distinct advantages of good stability and portability, tunable shape and size, real-time detection, non-invasion, extensive suitability in gas/vapor sensing, and recycling. In this review, we summarize the recent advances in luminescent MOF thin films, including the fabrication methods and origins of luminescence. Specifically, luminescent MOF thin films as biosensors for temperature, ions, gases and biomolecules are highlighted.

Keywords: metal–organic frameworks; thin films; preparation; luminescence; biomedical sensing

1. Introduction

The use of biosensors to detect and quantify the presence of targeted compounds is of great significance in diverse fields, such as medicine, pharmacology, agriculture and food safety, environmental monitoring, industry, defense, homeland security, etc. A biosensor is defined as a device with biological sensing elements connected to or integrated within a transducer [1,2]. Biosensors can employ a variety of transduction mechanisms, with luminescence-based sensors being the subject of this review. The luminescent biosensor utilizes changes in the photoluminescence of a fluorescent material induced by analyte-probe interactions or target conditions (e.g., temperature) to quantitate chemical/biological species [3,4]. Luminescent materials can be conjunct with spectrophotometers to identify the sensed material based on the characteristic absorption and emission shifts, and they can quickly and easily give a colorimetric response to stimuli [5,6]. The main advantages of fluorescence-based techniques over other transduction ones are ease of use, non-invasive, technical simplicity, and broad adaptability [7]. Recently, tremendous amounts of luminescent chemo-/bio-probes based on organic luminophores (e.g., small molecules, fluorescent conjugated polymers) [8–12] and inorganic luminophores (e.g., quantum dots and metal nanoclusters) [13,14] have been successfully developed. However, the organic luminophores often own an inherent hydrophobicity, and it is difficult to make them hydrophilic. The inorganic luminophores are often water-soluble and exhibit some congenital shortcomings: (1) inconvenience of store and transport; (2) nonrecycling since they are not easily separated from the analytes in solutions; (3) reagent consumption and environmental pollution; and (4) difficulty in detecting vapor/gas [15,16]. Additionally, these two types of probes have high biotoxicity, which hinders their extensive applications.

Development of film-based luminescent sensors can overcome the drawbacks of the above probes for chemo-/bio-sensing [15,17]. The luminescent films can be easily converted into a device format with several unique advantages: (1) luminescent films with any shape and size (depending on the substrate pattern) can be easily fabricated to meet various needs and occasions; (2) they are easy to store and transport; (3) there is no intrusive interference since the detection is usually carried out in the absence of external addition; (4) luminescent films enable the real-time detection of analytes; (5) luminescent films can be regenerated by washing with a suitable solvent; and (6) luminescent films have less damage to organisms because of the good chemical stability of luminophores in the solid state. Besides, the numbers of defects and grain boundaries in highly oriented quasi-epitaxial films are significantly reduced, and the numbers of binding sites at the outer surface of film are constant and do not depend on the thickness.

Metal–organic frameworks (MOFs), also known as porous coordination polymers (PCPs), which are constructed by the self-assembly of metal ions or clusters and organic ligands, have been widely explored as biosensors because of the unique luminescent properties, diverse advantages from structural and functional components, low biotoxicity, and easy preparation in thin films [18–20]. Specifically, MOF sensors have several key advantages over other potential luminescent probe materials: (1) MOFs possess immense potential for tunability and functionalization by altering the metal ions and organic ligands; (2) the inherent crystallinity of MOFs permits exact knowledge of the interactions that may be involved in the detection of analytes; (3) the porosity of MOFs can support the adsorption of analytes into the MOF pores, which can result in preconcentration of the analyte and close-interactions between the MOF and analyte species; (4) the porous frameworks allow the introduction of analyte-selective guest molecules through post synthetic modification into MOF structures for specific recognition. To date, luminescent MOF sensors have been successfully implemented for the detection of vapors/gases [21], explosive chemicals [22–25], ions [26–28], biomarkers [29–31] and temperature [32,33]. However, most of them are powdery sensors, which are difficult to operate and hard to recycle, severely limiting their biosensing applications. Fortunately, a variety of strategies, such as solution-based deposition, electrochemical deposition, and coating/casting, have been developed for fabricating MOF thin films. MOF film-based sensors not only retain the intrinsic sensory properties of the corresponding powdery MOFs, but also have the maneuverable nature of film, which shows a broad application prospect in the field of biosensing.

Nowadays, there are a lot of reviews on MOF-based luminescent probes [23,34–38] or the fabrication methods of MOF thin films [39–46]. However, there are no comprehensive reviews on luminescent MOF films for biosensing. In this review, we made such an effort to systematically review the progress of fabrication methods in designing various luminescent MOF films for biosensing. We firstly summarized the main methods for fabrication of MOF thin films followed by a brief introduction of the origins of MOF film luminescence. Finally, we focused on luminescent MOF thin films as biosensors for temperature, ions, gases and biomolecules, and demonstrated the sensory properties of such films that are related to their structures. This review would serve as a guide to better understand and cultivate the design strategies of luminescent MOF film sensors with high sensitivity, selectivity, stability and portability.

2. Methods for the Fabrication of MOF Thin Films

A number of synthetic strategies, including liquid-phase epitaxy (LPE), substrate-seeded heteroepitaxy (SSH), atomic layer deposition (ALD), bottom-up modular assembly (BMA), electrochemical deposition (ECD), and spin coating techniques (SCT), have been developed for the fabrication of MOF thin films. In this review, we divided them into three different categories: (1) deposition from solvothermal mother solutions, a method where a substrate is used (or modified by organic molecules) together with an appropriate growth solution containing the reactants, e.g., metal precursors and organic ligands, (2) electrochemical synthesis, which includes anodic deposition,

electrophoretic deposition and cathodic deposition and (3) mixed matrix membranes (MMMs), where essentially powders made using conventional solvothermal synthesis are coated onto a substrate.

It is needed to mention that an appropriate substrate and suitable surface modification are crucial for the deposition of MOF thin films, in particular for the deposition from solvothermal mother solution methods. Different types of substrates, such as planar solid (indium tin oxide (ITO), Si, Au, fluorine-doped tin oxide (FTO)), flexible (plastic, polystyrene fiber), and nonplanar substrates (metal oxide, porous metal), and substrates modified with different functional groups ($-\text{COOH}$, $-\text{NH}_2$, $-\text{OH}$, and $-\text{pyridine}$), have been widely studied for the deposition and support of MOF thin films [41]. These functional groups can be used to anchor the metal/metal-oxo nodes and organic linkers, thereby nucleating the growth of MOF thin films. Using different functional groups or tuning the density of functional groups, the growth orientation of MOF thin films can be systematically controlled and the highly oriented MOF thin films can be obtained under favorable conditions.

2.1. Deposition from Solvothermal Mother Solutions

Like the preparation of powdery MOF, the solvothermal method is a main method for preparing MOF thin films. In general, the synthesis of MOF thin films follows one of two approaches: in situ growth or seed-assisted (secondary) growth.

2.1.1. In Situ Growth

The most straightforward method of preparing an MOF thin film is inserting one or several substrate(s) into the mother solution of a given MOF following the usual solvothermal synthesis. The nucleation, growth and interchange of crystals on the substrate occur during the same preparation process. Growth occurs at the surface and sometimes also in solutions at the same time. This growth causes the crystals to adhere to the surface of the substrate in a more or less intergrown and continuous manner. Despite its superficial simplicity, this method can be quite powerful, especially for oxide wafers, metal slices, fibers, and even porous alumina in some cases. In this way, dense, crystalline and homogeneous thin films with micrometer-scale thickness have been obtained.

The first continuous and well-intergrown membrane, MOF-5 membrane, was prepared by Lai and Jeong et al. on a porous α -alumina without substrate modification by in situ solvothermal synthesis [47]. The porous α -alumina is placed in a solution of 1,4-terephthalic acid in DMF for half an hour, followed by addition of dehydrated $\text{Zn}(\text{NO}_3)_2 \cdot 0.86 \cdot \text{H}_2\text{O}$, and finally heated to 105°C for solvothermal reaction to obtain an MOF-5 membrane. Figure 1 shows that the continuous and dense MOF-5 membrane was successfully prepared and membranes with different thicknesses were obtained at different synthesis time or at different solvents. Besides MOF-5, other MOF membranes, such as $\text{Cu}_3(\text{btc})_2$ (btc = 1,3,5-benzenetricarboxylate) [48], $\text{Zn}(\text{bdc})_2(\text{dabco})$ (bdc = 1,4-benzenedicarboxylate; dabco = 1,4-diazabicyclo[2.2.2]octane) [48], ZIF-8 [49], were also successfully prepared on porous alumina by the same method.

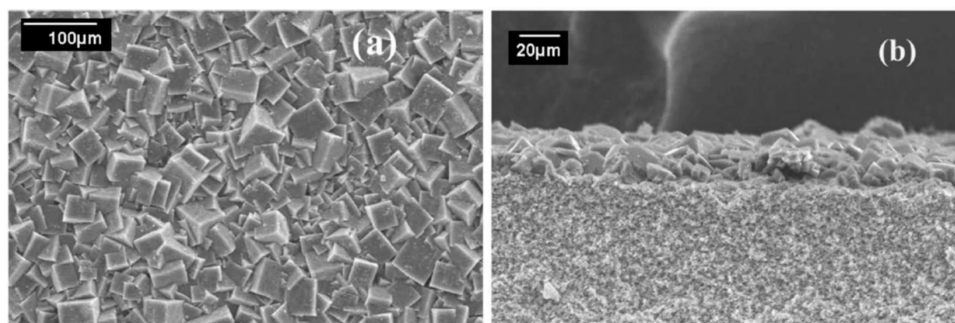


Figure 1. SEM images of the MOF-5 membrane: (a) top view; (b) cross section. Reprinted with permission from Reference [47]. Copyright 2009 Elsevier.

In addition, a dense ZIF-8 membrane with a thickness of approximately 50 μm is directly fabricated on the porous TiO_2 substrate by the microwave heating in situ solvothermal method [50]. Other substrates were also used for deposition of MOF films, and continuous HKUST-1 and ZIF-8 thin films were obtained in silicon slices [51].

However, it is still difficult to prepare continuous MOF membranes on unmodified supports because the heterogeneous nucleation of MOF crystals on support surfaces is not homogeneous and efficient. In addition, MOF grains formed in solutions are difficult to adhere to the surface of the substrate due to the lack of binding sites. There are two main strategies to promote the growth of MOF grains on the substrate and increase the interaction of the MOF thin films with the substrate: “metal source” and substrate surface modification.

The synthesis of MOFs involves the coordination of metal centers with organic ligands, and it is particularly favorable when the substrate is made of the same metal as the MOF. Under the guidance of this idea, Qiu and Zhu et al. successfully produce an HKUST-1 thin film using the “twin copper source” method (Figure 2) [52]. In the in situ solvothermal growth process, the oxidized copper net and the Cu^{2+} in a mother solution provide the metal source for the growth of MOF crystals. At the same time, the oxidized copper net provides a homogeneous nucleation site for the growth of a continuous and dense MOF membrane. In addition, the same group prepared a $\text{Zn}_3(\text{BTC})_2$ thin film by placing an H_2O_2 -activated zinc sheet in the aqueous solution of H_3BTC [53]. In 2011, Martens et al. produced a continuous $\text{Cu}_3(\text{BTC})_2$ thin film by an in situ hydrothermal reaction using oxidized copper as a substrate [54]. Furthermore, a simple method of ‘single nickel source’ has been developed by Qiu and Xue et al. to prepare a homochiral $\text{Ni}_2(\text{L-asp})_2(\text{bipy})$ (L-asp = L-aspartic acid, bipy = 4,4'-bipyridine) membrane (Figure 3) [55]. The nickel net plays a dual role in the synthesis process as the only nickel source and as a substrate supporting the membrane. Because the nickel net is the only metal source in the reaction system, the growth process stops once a layer of the crystal film is formed, making the final membrane thinner and continuous.

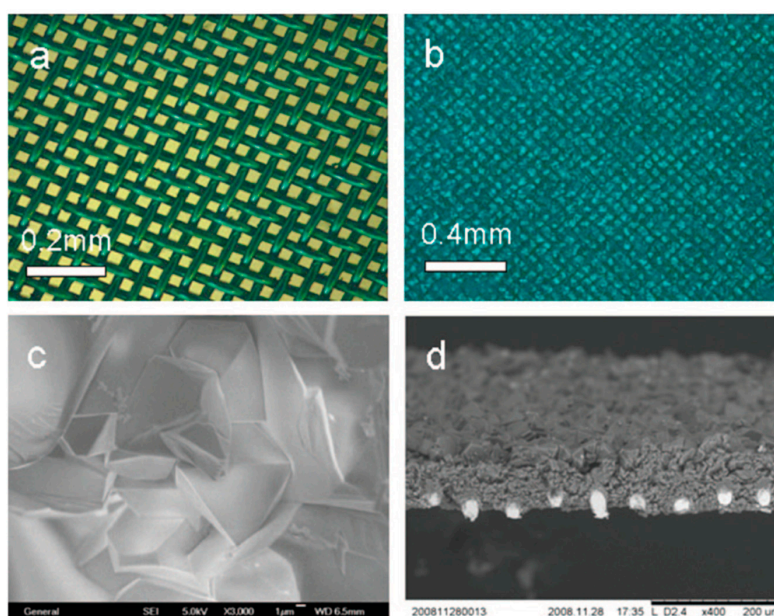


Figure 2. Optic micrographs of the (a) copper net and (b) net-supported $\text{Cu}_3(\text{BTC})_2$ membrane; SEM images of (c) the surface and (d) a cross section of the membrane. Reprinted with permission from Reference [52]. Copyright 2009 the American Chemical Society, (Washington, DC, USA).

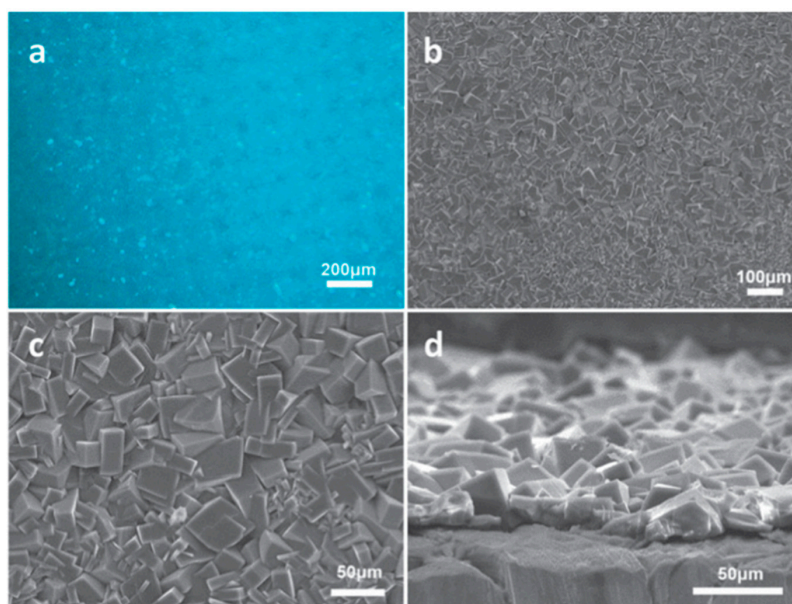


Figure 3. Leica picture of (a) the $\text{Ni}_2(\text{L-asp})_2(\text{bipy})$ membrane; SEM pictures of (b,c) surface and (d) a cross section of the $\text{Ni}_2(\text{L-asp})_2(\text{bipy})$ membrane. Reprinted with permission from Reference [55]. Copyright 2013 the Royal Society of Chemistry, (London, UK).

Poor bonding of the MOF thin films to the substrates is a common challenge. In order to improve the bonding force between the MOFs film and the substrate, functional surface modification of the substrate becomes a powerful means. Huang and Caro et al. report a covalent functionalization strategy to prepare ZIF-90 and ZIF-22 membranes by using 3-aminopropyltriethoxysilane (APTES) as covalent linkers between the MOF layers and supports' surfaces [56,57]. Figure 4 shows the amination of a porous Al_2O_3 substrate and the preparation of ZIF-90 polycrystalline film. In the first step, the ethoxy groups of the APTES react with the hydroxyl groups on the surface of Al_2O_3 support. In the second step, the amino groups react with the aldehyde groups of imidazole-2-carboxaldehyde via imines condensation, and then the nucleation and crystal growth of the ZIF-90 start at these fixed sites on the surface of the porous ceramic supports. After solvothermal reaction for 18 h at $100\text{ }^\circ\text{C}$, the ZIF-90 layer is completely covered by the surface of the APTES modified support with a thickness of about $20\text{ }\mu\text{m}$. In the growth process of the ZIF-22 polycrystalline film, their group believes that the amino groups in 3-aminopropyltriethoxysilane can be coordinated with Zn^{2+} , thus connecting the ZIF-22 nanocrystals and the substrate, and finally forming a dense ZIF-22 polycrystalline film [57]. Modifying the surface of porous α -alumina and porous potassium hexatitanate with hydroxyl groups, as well as modifying the surface of silicon with carboxy groups by self-assembled monolayer (SAM), continuous and dense $\text{Zn}_2(\text{bdc})_2(\text{dabco})$, $\text{Mn}(\text{HCOO})_2$ and HKUST-1 polycrystalline films are successfully prepared [58,59].

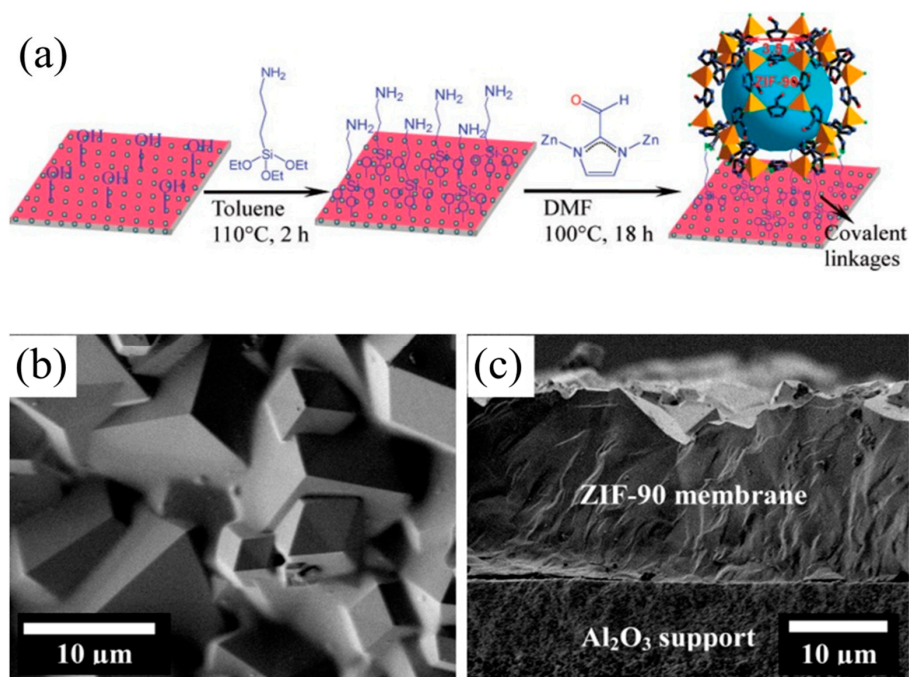


Figure 4. (a) Scheme of the preparation of ZIF-90 membrane via imine condensation reaction with 3-aminopropyltriethoxysilane (APTES) as a covalent linker; SEM images of (b) a top view and (c) a cross section of the resulted ZIF-90 membrane. Reprinted with permission from Reference [56]. Copyright 2010 the American Chemical Society, (Washington, DC, USA).

2.1.2. Seed-Assisted Growth

Seeded growth, also known as secondary growth, is a process, in which a seed layer is coated or deposited on a substrate and then on deposited MOF thin films under solvent or hydrothermal conditions. Due to the low heterogeneous nucleation density of many MOF crystals on the porous ceramic carrier substrates, this method is widely used to prepare dense and packed MOF thin films. Seeded growth allows for more effective control of crystal growth and orientation of MOF membranes, and it requires two steps: preparation and deposition of seeds followed by growth into a film. Various materials, such as MOF nanocrystals, non-MOF particles, coordination polymers, even MOF thin films, can be used as seeds [60,61].

Very recently, Qian and Cui et al. developed a strategy, named “in situ secondary growth”, to fabricate a Eu-BDC-NH₂ film on common glass with a UiO-66-NH₂ layer as seed layers [62]. Because of the matched components and structures of Eu-BDC-NH₂ and UiO-66-NH₂, the Eu-BDC-NH₂ film can be successfully fabricated on the UiO-66-NH₂ layer through in situ secondary growth. The space groups of UiO-66-NH₂ and Eu-BDC-NH₂ are *F43m* and *Fm3m*, respectively. These similar crystal structures and the same ligand avoid the mismatch between the lattices and components. As shown in Figure 5, a common glass with abundant hydroxylate on the surface is obtained by treating with the piranha solution. The well-intergrown UiO-66-NH₂ with the thickness of about 1 μm is formed on the treated glass after solvothermal synthesis (Figure 6a,c). Then, the washed UiO-66-NH₂ film is vertically put into the mother solution of Eu-BDC-NH₂ and heated to 120 °C for 24 h. After the in situ secondary growth, the observed Eu-BDC-NH₂ grains have a size of around 1–2 μm, and tightly cohere to each other, leading to a crack-free film of around 2 μm in thickness (Figure 6b,d). The [Cu(ndc)(dabco)_{0.5}] (ndc = 1,4-naphthalenedicarboxylate, dabco = 1,4-diazabicyclo[2.2.2]octane) film with itself as seed layers and IRMOF-3 film with MOF-5 as seed layers are reported by Yusenko et al. and Yoo et al., respectively [63,64].

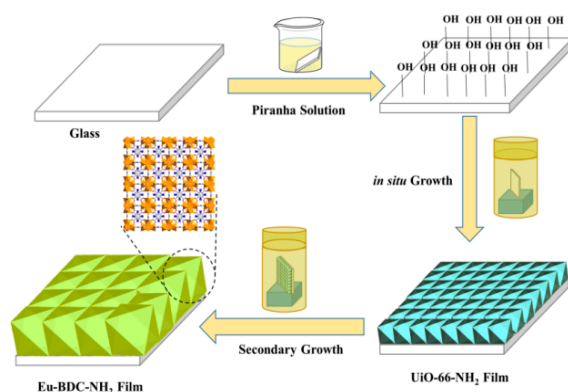


Figure 5. Synthetic route of a Eu-BDC-NH₂ film by an in situ secondary growth method with a UiO-66-NH₂ film as the seed layers. Reprinted with permission from Reference [62]. Copyright 2018 Elsevier.

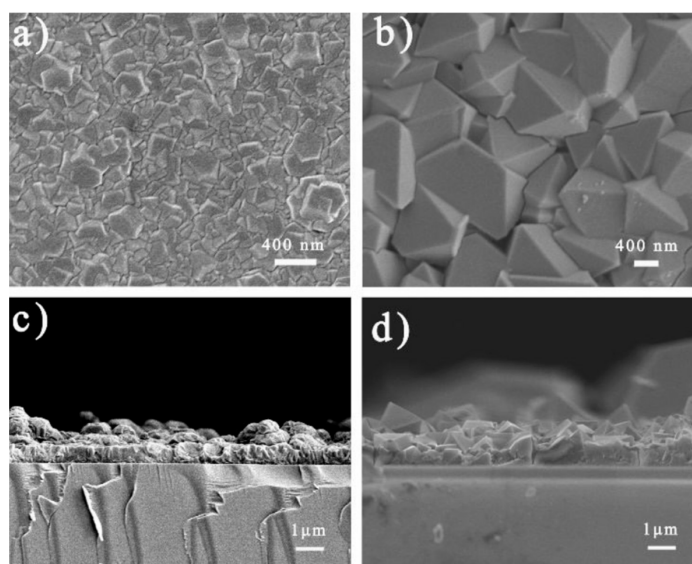


Figure 6. SEM images of (a) a top view and (c) a cross section of UiO-66-NH₂ film; SEM images of (b) a top view and (d) a cross section of Eu-BDC-NH₂ film. Reprinted with permission from Reference [62]. Copyright 2018 Elsevier.

Takahashi and Falcaro et al. demonstrate that the substrate-seeded heteroepitaxy approach can permit the fabrication of large-scale epitaxial MOF thin films with unrestricted substrate size and rigidity [65]. The oriented microcrystalline Cu(OH)₂ nanobelts are used as a source of metal ions, and a substrate-seeded heteroepitaxial growth of Cu₂(BDC)₂ thin film is rapidly fabricated (Figure 7). After immersing the Cu(OH)₂ nanobelt film in a saturated ethanolic solution of H₂BDC, a continuous Cu₂(BDC)₂ MOF film orthogonal to the nanobelts is observed within 5 minutes (see Figure 7e,f). Out-of-plane XRD measurements and in-plane XRD measurements confirm that the (h00) and (0k0) faces of the MOF crystals are aligned and precisely oriented along the metal hydroxide crystallographic directions. Together with the transmission electron microscope (TEM) analyses, the epitaxial Cu₂(BDC)₂ thin film is determined to crystallize in *P2* symmetry with lattice parameters ($a = 10.90 \text{ \AA}$, $b = 5.89 \text{ \AA}$, and $c = 10.90 \text{ \AA}$), which are excellently matched with the Cu(OH)₂ nanotubes with *P4* symmetry and lattice parameters ($a = 10.61 \text{ \AA}$, $b = 5.80 \text{ \AA}$, and $c = 10.61 \text{ \AA}$), as shown in Figure 7c,d. In addition, since the size and rigidity of the substrate are essentially unrestricted, the substrate-seeded heteroepitaxy approach allows the fabrication of flexible and large-scale MOF thin film-based devices (Figure 7g,h).

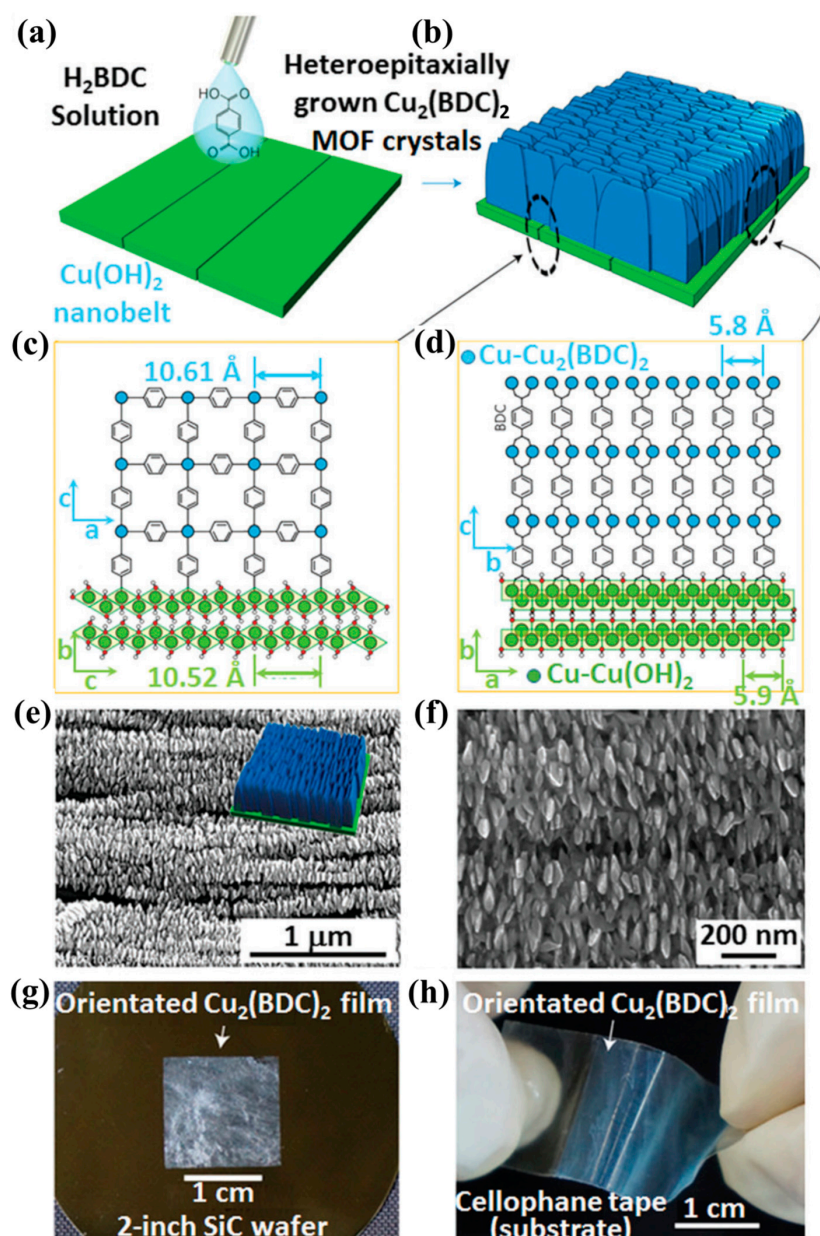


Figure 7. Substrate-seeded heteroepitaxial growth of the $\text{Cu}_2(\text{BDC})_2$ film on oriented microcrystalline $\text{Cu}(\text{OH})_2$ nanobelts. (a) Ligand (H_2BDC)-containing solution is placed in contact with the $\text{Cu}(\text{OH})_2$ nanobelt; (b) $\text{Cu}_2(\text{BDC})_2$ MOFs are heteroepitaxially grown on the aligned $\text{Cu}(\text{OH})_2$ nanobelt; (c,d) Crystal structures of both $\text{Cu}(\text{OH})_2$ and $\text{Cu}_2(\text{BDC})_2$ MOFs; (e,f) SEM images of $\text{Cu}_2(\text{BDC})_2$ MOFs epitaxially grown on aligned $\text{Cu}(\text{OH})_2$ nanobelt films; (g) $\text{Cu}_2(\text{BDC})_2$ MOF films on a SiC wafer; (h) Aligned $\text{Cu}_2(\text{BDC})_2$ MOFs deposited on a flexible cellophane tape. Reprinted with permission from Reference [65]. Copyright 2017 the Nature Publishing Group, (London, UK).

2.2. Electrochemical Synthesis

Electrochemical synthesis of HKUST-1 thin films was first introduced by researchers at Badische Anilin-und-Soda-Fabrik (BASF) [66]. Since then, scientists have done a lot of research in the electrochemical preparation of high-quality MOF films [67,68]. Three main approaches have been described for the fabrication of MOF thin films via electrochemical methods: (1) anodic deposition, (2) electrophoretic deposition, and (3) cathodic deposition (Figure 8) [41,67].

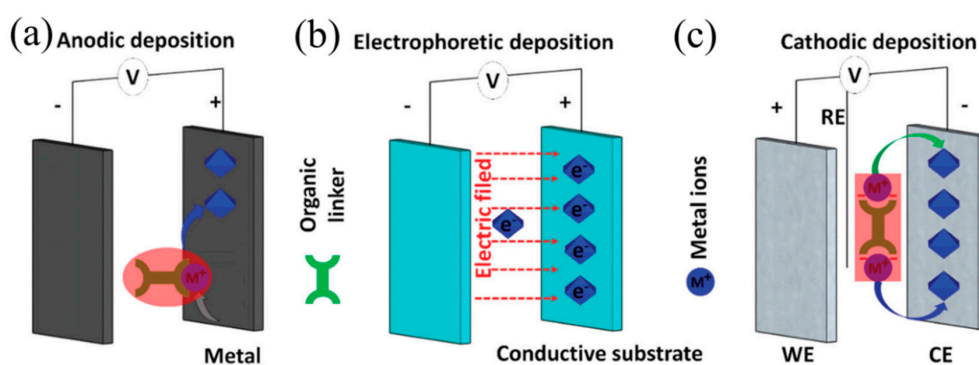


Figure 8. Schematic representation of the electrochemical synthesis of MOF thin films with (a) anodic deposition; (b) electrophoretic deposition and (c) cathodic deposition. Reprinted with permission from Reference [41]. Copyright 2017 the Royal Society of Chemistry, (London, UK).

In the anodic deposition process (Figure 8a), a metallic electrode is electrochemically oxidized to provide metal ions, and MOF thin films grow on the anode when the electrochemically generated metal ions react with the organic linkers contained in the electrolyte. Ameloot et al. showed that, by carefully optimizing the conditions and in the absence of stirring, the anodic deposition method can be used to grow HKUST-1 on copper anodes [69]. The HKUST-1 layer is formed in 30 min or less by applying an anode voltage to the copper electrode immersed in a BTC solution. Various thicknesses (2–50 μm) and intergrowth degrees could be obtained by variation of the water content of the solution as well as the voltage and frequency of the applied tension. Since metal ions are provided on the surface where nucleation occurs, crystals and the resulting film are highly homogeneous. To the best of our knowledge, various types of MOF thin films, such as $\text{Zn}_3(\text{BTC})_2$ on Zn plates [70], MIL-100(Fe) on Fe anodes [71], and Zn(TPTC) on Zn plates [72], have also been fabricated by this method.

In the electrophoretic deposition process (Figure 8b), two conductive electrodes are immersed in solutions containing surface-charged MOF particles. When a voltage is applied between the two electrodes, the resulting electric field drives the MOF particles toward the oppositely charged electrode, thus leading to the formation of MOF thin films. The electrophoretic deposition method is well suited to the facile and rapid fabrication of MOF films on the traditional substrates, such as ITO and FTO glass and metal plates. HKUST-1, Al-MIL-53, UiO-66, NU-1000, carbon quantum dots (C-QDs)@UiO-66-(COOH)₂, Ln@UiO-66, Eu-NDC and so on, have been successfully fabricated with the electrophoretic deposition method [73–75].

During the cathodic deposition process (Figure 8c), two inert electrodes (WE, working electrode; CE, counter electrode) are used as chemically inert separators [76,77]. They are the only source of electrons and do not participate in the MOF-forming reactions. The key step in cathodic deposition is to obtain a local alkaline region near the cathode where the organic ligands are deprotonated. The “deprotonated” organic ligands react with metal precursors in solutions, inducing the crystallization of MOF particles at the cathode surface and forming MOF thin films.

2.3. Mixed Matrix Membranes

There are several possibilities for fabricating MOF thin films from essential powders made using conventional solvothermal synthesis: (1) direct deposition of powdered MOFs onto a substrate by drop-casting or spin-coating methods; (2) coating of an MOF particle suspension containing an additional polymeric binder to obtain MOF-based mixed matrix membranes (MMMs). Eddaoudi et al. implemented the spin-coating method to construct various MOF thin films, ranging in thickness from a few micrometers down to the nanometer scale including $\text{Cu}_2(\text{bdc})_2 \cdot x\text{H}_2\text{O}$, $\text{Zn}_2(\text{bdc})_2 \cdot x\text{H}_2\text{O}$, HKUST-1, and ZIF-8 [78]. Zhang et al. synthesize a continuous and smooth lanthanide MOF films, $\text{Eu}_{1-x}\text{Tb}_x\text{-MOF}$, via spin-coating deposition [79]. Similarly, MIL-101(Cr) and MIL-101(Cr)-NH₂ films are

prepared on alumina supports by Burrows et al. with the polyethylenimine (PEI)-assisted dip-coating method [80,81].

Besides, given the vast possibilities that MOFs offer in terms of design together with their intrinsic hybrid nature, research into MOF-based MMMs has experienced an unprecedented explosion since the first report in 2004 [82–85]. The lab-scale manufacture of MOF-based MMM is similar to the one applied for the synthesis of other MMMs [86]. In the general procedure, the first step is the dispersion of powdery MOFs in the solvent in an ultrasonic bath. A polymer (such as polymethyl methacrylate, PMMA; polyvinylidene fluoride, PVDF; polyacrylonitrile, PAN) is then added. The whole mixture is stirred overnight. Before the casting, different intervals of sonication and stirring take place to ensure good dispersion. Subsequently, the membranes are cast on a flat surface, and then left overnight for evaporation of solvent at room temperature. Once dried, the films are placed in a vacuum oven for 24 h at a specific temperature (depending on the polymer glass transition temperature) high enough to remove the remaining solvent.

In a recent paper, Cohen et al. achieve the integration of a wide range of MOF particles (UiO-66, UiO-66-NH₂, MIL-101(Cr), MIL-101(Fe), HKUST-1, MIL-53(Fe), ZIF-8) in an MMM with a high MOF content (≈ 67 wt %) (see Figure 9a) [87]. These synthesized MMMs retain high specific surface areas of the parent MOFs and readily undergo post-synthetic modification (PSM) and post-synthetic exchange (PSE) producing. In addition, these MMMs can be fabricated on a large scale and are easy to handle and manipulate (Figure 9b).

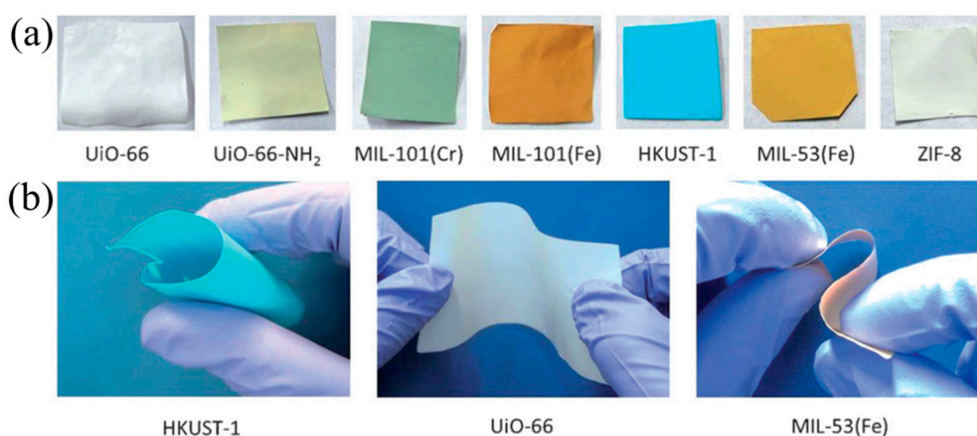


Figure 9. (a) Free-standing mixed matrix membranes (MMMs, $\approx 1 \times 1 \text{ cm}^2$) produced from a variety of MOFs; (b) Flexibility of large-area HKUST-1, UiO-66, and MIL-53(Fe) MMMs ($\approx 3 \times 5 \text{ cm}^2$). Reprinted with permission from Reference [87]. Copyright 2015 WILEY-VCH Verlag GmbH & Co. (Weinheim, Germany).

Detailed SEM images of a UiO-66 MMM with an MOF content of about 67 wt % are shown in Figure 10. The octahedral UiO-66 microcrystals clearly remain intact and are well integrated with the polymer binder. The torn edge of MMM in Figure 10b highlights the integration of UiO-66 crystals with the polyvinylidene fluoride (PVDF) strands. The MOF particles are densely packed within the film with approximately 35 nm in thickness.

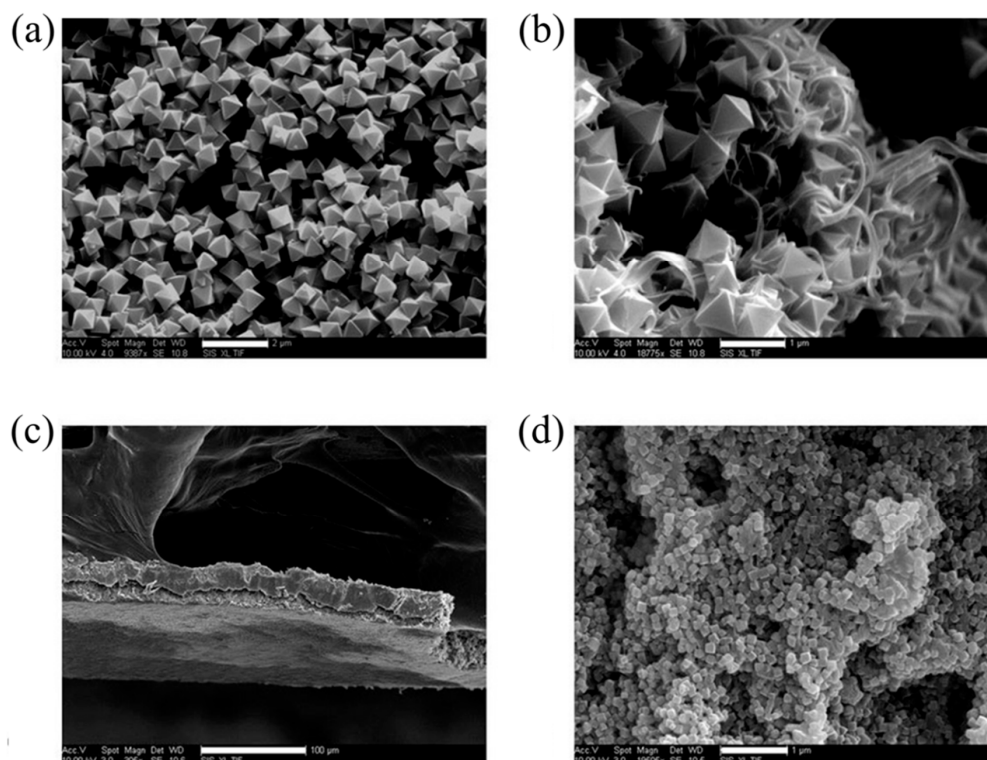


Figure 10. SEM images of (a,b) a top view and (c,d) a cross section of UiO-66 MMM. Scale bars: (a): 2 μm ; (b,d): 1 μm ; (c): 100 μm . Reprinted with permission from Reference [87]. Copyright 2015 WILEY-VCH Verlag GmbH & Co., (Weinheim, Germany).

3. Luminescence Behavior in MOF Thin Films

The ability to load a deposited MOF thin layer with luminescent materials provides many interesting options. The most obvious one is to check morphology and texture of the deposited MOF film, e.g., to check for holes, incompletely covered areas, cracks, scratches and even to determine the thickness. In addition, the luminescent MOF thin films open up the possibility to use such materials for optical data storage, color displays, luminescence detecting and mapping. Like the powdery MOFs, luminescence of MOF thin films can generate from the luminescent metal ions or clusters, organic ligands, and charge-transfer, such as ligand-to-metal charge transfer (LMCT) and metal-to-ligand charge transfer (MLCT), as well as the loaded guest molecules.

3.1. Lanthanide Luminescence

In the past decades, lanthanide MOF thin films have attracted extensive attention due to their unique luminescence properties, such as high luminescence quantum yield, long-lived emission, large Stokes shifts, and characteristically sharp line emissions. Most of the reported luminescent MOF thin films are based on lanthanide luminescence. Due to the parity-forbidden $f-f$ transitions, it is hard to yield strong luminescence with direct excitation of the lanthanide ions. The luminescence of lanthanide ions is often generated from the energy transfer processes, known as “luminescence sensitization” or “antenna effect” [88,89]. The mechanism of luminescence sensitization within lanthanide MOF thin films is comprised of three steps: (1) light is absorbed by the organic ligands around the lanthanide ions; (2) energy is transferred to the lanthanide ions from organic ligands; and (3) luminescence is generated from the lanthanide ions.

In 2010, Zhang et al. synthesized a continuous and smooth lanthanide MOF film with high mechanical stability via spin-coating deposition [79]. In this study, they first synthesize a series of shape-and-size adjustable bimetallic Ln-MOFs nanocrystals by the capping method. The nanometer-sized crystals are

then used to deposit continuous and smooth $\text{Eu}_{1-x}\text{Tb}_x\text{MOF}$ thin films on ITO-coated glass substrates with spin-coating deposition. The fabricated films show strong luminescence of Eu^{3+} and Tb^{3+} , and are characterized by an efficient Tb^{3+} -to- Eu^{3+} energy transfer (see Figure 11). Since then, different types of lanthanide MOF films, such as europium-based MOF films, terbium-based MOF films, and mixed lanthanide MOF films, have been reported [90–92].

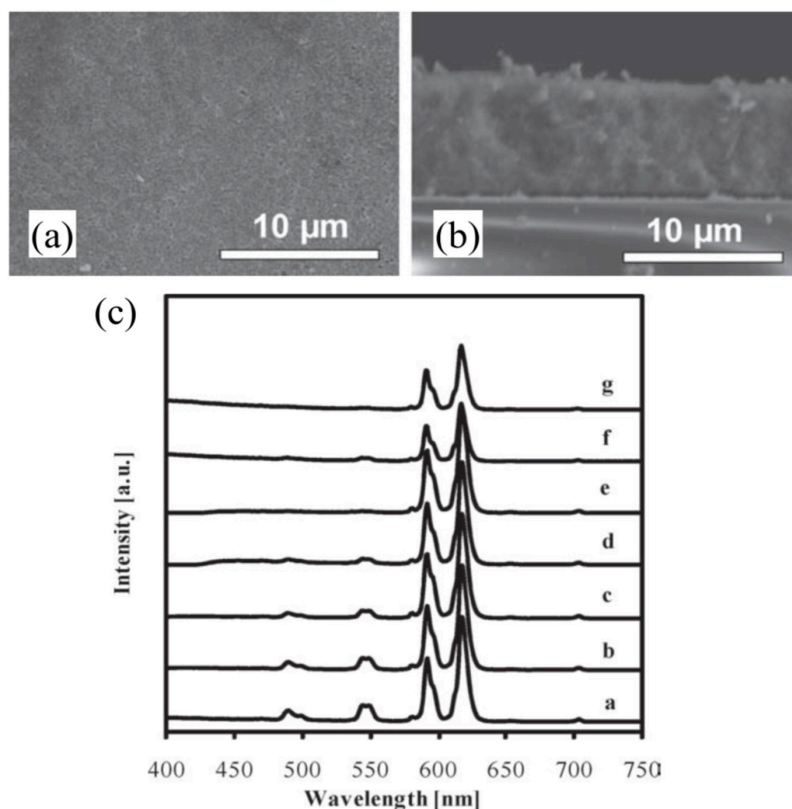


Figure 11. SEM images of a $\text{Tb}_{0.5}\text{Eu}_{0.5}\text{-MOF}$ film viewed from: (a) the surface and (b) the cross section; (c) Spectra of luminescent $\text{Eu}_{1-x}\text{Tb}_x\text{-MOF}$ films with different $\text{Tb}^{3+}/\text{Eu}^{3+}$ mole ratios: a, 2.75; b, 2.44; c, 1.95; d, 1.46; e, 1.02; f, 0.40; g, 0.30. Reprinted with permission from Reference [79]. Copyright 2010 WILEY-VCH Verlag GmbH & Co., (Weinheim, Germany).

3.2. Ligand-Based Luminescence

The ligand-based luminescence is usually observed in two cases: (1) transition-metal-based MOF films, such as zirconium-based and zinc-based MOF films; (2) lanthanide-based MOF films with insufficient antenna sensitization.

Qiu and Zhu et al. synthesize an MOF $\text{Zn}_3(\text{BTC})_2$ film on the substrate of zinc wafer by a direct conversion technique [53]. The reaction between the substrate-generated zinc source and the H_3BTC solution yields the inter-growth of crystals, and then forms a compact and continuous $\text{Zn}_3(\text{BTC})_2$ film. Upon excitation at 327 nm, $\text{Zn}_3(\text{BTC})_2$ film exhibits a strong and broad emission of ligand with the peak at about 390 nm, and the fluorescence property of $\text{Zn}_3(\text{BTC})_2$ film is utilized to detect dimethylamine.

In lanthanide-based MOF films, if antenna sensitization is not very efficient, both remaining ligand fluorescence and the lanthanide-centered luminescence can be observed [93]. In addition, if the amount of energy acceptor (lanthanide ions) is not high enough, the fluorescence of the ligand is strong and obvious. Recently, Cao et al. reported a Tb@UiO-66-Hybrid film, featuring with two typical emission peaks of ligand and lanthanide ions upon excitation at 330 nm (Figure 12) [75]. The peak at 430 nm is derived from the ligand (H_2NDC). In addition, the peaks at 489, 544, 584, and 620 nm ($^5\text{D}_4\text{-}^7\text{F}_j$, $J = 6, 5, 4, 3$) correspond to characteristic Tb^{3+} emissions. Similarly, the Eu@UiO-66-Hybrid

film features two typical emissions based on the ligand (H₂NDC) and Eu³⁺ with characteristic sharp lines at 578, 592, 616, 650, and 699 nm (⁵D₀-⁷F_J, J = 1, 2, 3, 4). The dual-emitting Tb@UiO-66-Hybrid and Eu@UiO-66-Hybrid films are further applied to detect temperature changes.

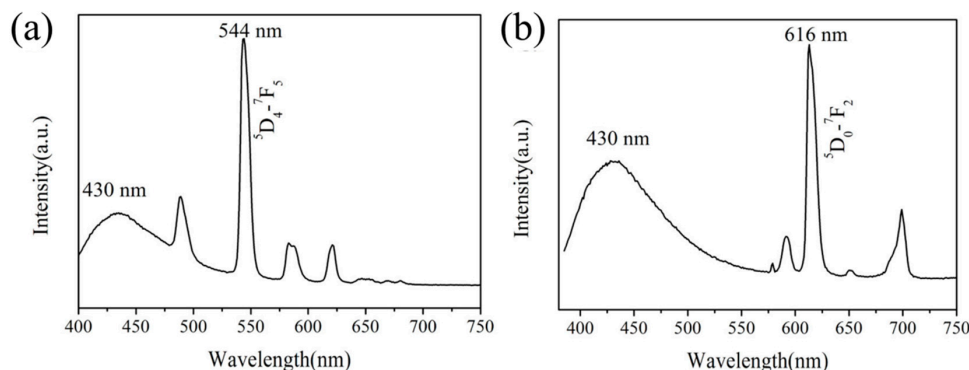


Figure 12. Emission spectra of Tb@UiO-66-Hybrid (a) and Eu@UiO-66-Hybrid (b) films excited at 330 nm. Reprinted with permission from Reference [75]. Copyright 2018 the American Chemical Society, (Washington, DC, USA).

3.3. Luminescence Generated from Guest Molecules

Because of the highly regular channel structures, controllable pore sizes and abundant modifiable sites, the MOF films can serve as hosts for the encapsulation of the guest luminescent species, such as lanthanide ions/complexes, fluorescent dyes and fluorescent quantum dots. Qian and Cui et al. introduced the Tb³⁺ ions into the two indium MOF films, [(CH₃)₂NH₂][In₃O(BTC)₂(H₂O)₃]₂[In₃(BTC)₄] (CPM-5) and In₃O(OH)(H₂O)₂[BTC]₂ (MIL-100(In)) through the post-functionalization [94]. The presence or absence of extra carboxylate acid in these two films makes adjustment on energy transfer processes and thereby oxygen sensitivities possible. Recently, MIL-124@Eu³⁺ film was successfully prepared via post-synthetic modification of the MIL-124 film with europium ions by the same group [95].

Besides lanthanide ions, small lanthanide complexes can be encapsulated into the pores of MOF films. Europium chelate [Eu(bzac)₃bipy] (bzac = 1-benzoylacetone, bipy = 2,2'-bipyridine) is loaded into a three-dimensional (3D) porous MOF film, HKUST-1 by Wickleder and Woll et al. (Figure 13) [96]. The loading process is carried out by immersion of the deposited MOF films into ethanolic solutions of Eu(bzac)₃bipy. XRD data recorded reveals the loading process does not destroy the porous framework. Room-temperature emission spectra of powdered Eu(bzac)₃bipy and powdered Cu₃(btc)₂-MOF loaded with Eu(bzac)₃bipy reveal that optical excitation can be transferred from the MOF ligands to the Eu-atoms embedded in the MOF pores.

In recent years, fluorescent C-QDs@MOFs composites have attracted the attention of scientists for display lighting, fluorescence imaging, and chemical sensing. Cao et al. employ a UiO-66 based MOF, UiO-66-(COOH)₂ with uncoordinated carboxylic group, to load the C-QDs (Figure 14) [74]. UiO-66-(COOH)₂ MOFs can absorb C-QDs from the solution and prevent C-QDs from aggregating, and the well-dispersed C-QDs impart fluorescence characteristics to composites. C-QDs@UiO-66-(COOH)₂ composites are deposited on zinc plates by electrophoretic deposition. In addition, different kinds of guest luminescent molecules (Eu³⁺ and C-QDs) can be loaded simultaneously and the resulted Eu@C-QDs@UiO-66-(COOH)₂ exhibits white fluorescence in the temperature range from 77 to 363 K upon excitation of 365 nm.

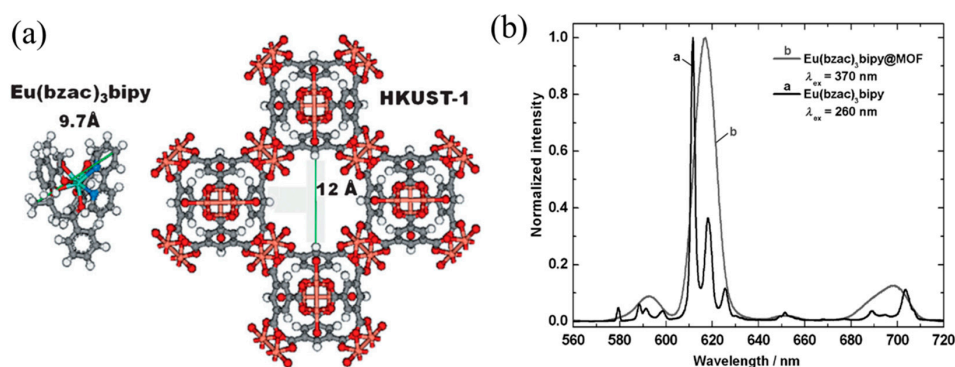


Figure 13. (a) Size of $\text{Eu}(\text{bzac})_3\text{bipy}$ and pore size of HKUST-1; (b) Room-temperature emission spectra of powdered $\text{Eu}(\text{bzac})_3\text{bipy}$ and powdered $\text{Cu}_3(\text{btc})_2\text{-MOF}$ loaded with $\text{Eu}(\text{bzac})_3\text{bipy}$. Reprinted with permission from Reference [96]. Copyright 2012 WILEY-VCH Verlag GmbH & Co., (Weinheim, Germany).

4. Biomedical Sensing Application of Luminescent MOF thin Films

To date, various types of luminescent MOFs have been reported and realized in sensing of metal ions, anions, gas molecules, nitro explosives, small molecules and temperature [21–33]. However, most of them are brittle crystals or loose powders synthesized by hydrothermal/solvothermal methods, which require specific solvent conditions to detect analytes. The operation is difficult and seriously limits their practical in-field applications. MOF thin films grown on solid substrates have many advantages over powdery and solution-based samples, such as: they are easily separated from liquid media; the numbers of defects and grain boundaries of highly oriented quasi-epitaxial layers are obviously reduced; and the numbers of binding sites at the outer surface of the MOF film are constant and do not depend on the thickness of MOF film. In the following section, we will discuss the luminescent MOF thin films as biosensors for detecting temperature, ions, gases and biomolecules, and some related powdery probes are also mentioned.

4.1. Temperature Sensing

Temperature is a critical parameter in both scientific research and industry. Since the first MOF-thermometer [$\text{Eu}_{0.0069}\text{Tb}_{0.9931}\text{-DMBDC}$] (H_2DMBDC = 2,5-dimethoxy-1,4-benzenedicarboxylic acid) was reported by Chen and Qian et al. [97], MOF-based luminescence thermometers have drawn great attention [98,99]. By designing a thin film of such a luminescence thermometer on a suitable substrate, a novel device can be developed, with which the surface temperature distribution can be easily mapped via a non-invasive method. Recently, Cao et al. prepared two Ln@UiO-66-Hybrid films and studied their temperature detection performances [75]. The smooth and uniform MOF films with a thickness of approximately 50 μm are fabricated by stepwise PSE and PSM, followed by the electrophoretic deposition method on unmodified FTO glass (Figure 15a,b). The Tb@UiO-Hybrid film features two typical emission peaks: the peak at 430 nm is derived from the ligand (H_2NDC), and the peaks at 489, 544, 584 and 620 nm correspond to characteristic Tb^{3+} emissions. Similarly, the Eu@UiO-66-Hybrid film features two typical emissions based on the ligand (H_2NDC) and Eu^{3+} with characteristic sharp lines at 578, 592, 616, 650 and 699 nm. When the temperature gradually increases from 303 to 403 K, the intensity at 430 nm in the Eu@UiO-66-Hybrid film decreases by about 15% of pristine intensity, while the intensity at 616 nm based on the europium ions gradually increases by approximately 2.5 times of pristine intensity (Figure 15c,d). There is a good function relationship between the intensity ratio at 613–430 nm and temperature with a relative sensitivity of $4.26\% \text{ K}^{-1}$ in the temperature range of 303–403 K (Figure 15e). In addition, the Tb@UiO-66-Hybrid film exhibit good temperature sensing properties with a relative sensitivity of $2.76\% \text{ K}^{-1}$ in the temperature range of 303–353 K. In a recent article, the same group reported a C-QDs functionalized MOF composite film C-QDs@UiO-66-(COOH)₂ film, which is also fabricated by the electrophoretic deposition method.

Based on the emission of C-QDs, this film can detect temperature in the range of 97–297 K with a relative sensitivity of $1.3\% \text{ K}^{-1}$ at 297 K.

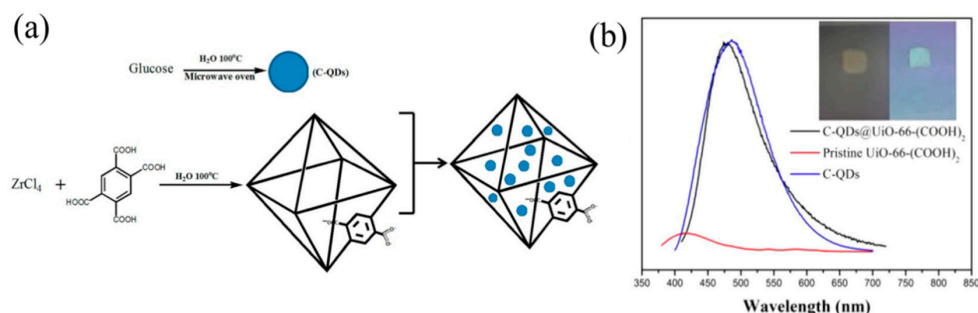


Figure 14. (a) Fabrication of C-QDs@UiO-66-(COOH)₂ (C-QDs = carbon quantum dots) composite; (b) Photoluminescence (PL) emission spectra of C-QDs, C-QDs@UiO-66-(COOH)₂, and UiO-66-(COOH)₂ dispersed in a water solution excited at 365 nm. Reprinted with permission from Reference [74]. Copyright 2018 the American Chemical Society, (Washington, DC, USA).

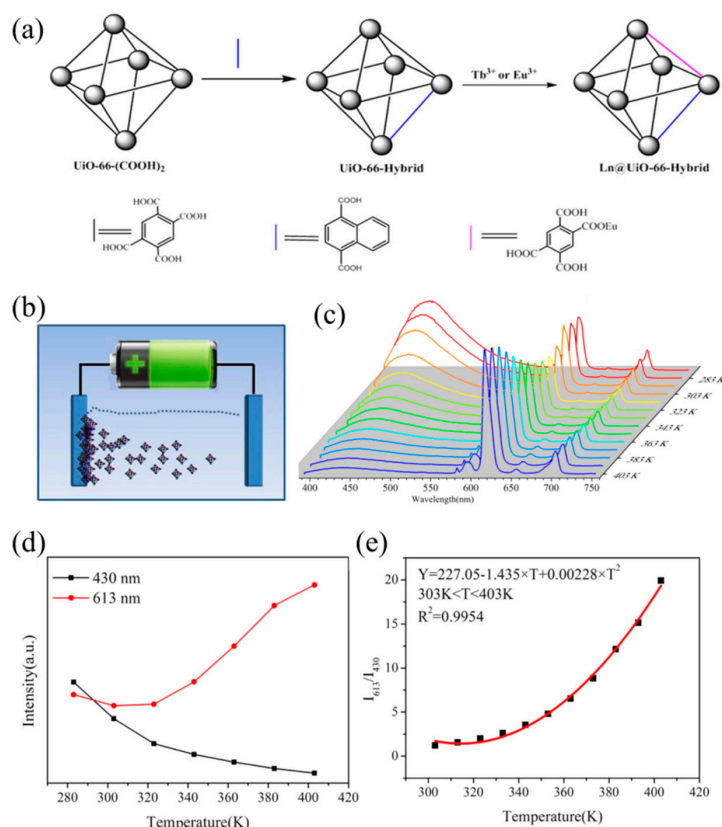


Figure 15. (a) Preparation of Ln@UiO-66-hybrid composition by post-synthetic exchange and post-synthetic modification; (b) Fabrication of composite films via electrophoretic deposition method; (c) Emission spectra of the Eu@UiO-66-hybrid in the temperature range of 273–403 K; (d) Emission intensities at 430 and 613 nm in the temperature range of 303–403 K; (e) Emission intensity ratio of the Eu@UiO-66-hybrid film as a function of temperature with the fitting curve. Reprinted with permission from Reference [75]. Copyright 2018 the American Chemical Society, (Washington, DC, USA).

Other groups have also reported some types of MOF film thermometers. Yan et al. fabricate a polymer hybrid thin film based on rare earth complexes RE(BPDC)(Ad) (BPDC = biphenyl-4,4'-dicarboxylic acid, Ad = adenine) via polymerization reaction of ethyl methacrylate (EMA) and 4-vinylpyridine (VPD) [100].

The resulted polymer thin film can act as a luminescent thermometer based on the energy transfer from Tb^{3+} to Eu^{3+} . With the one-step direct solvothermal synthesis method, Bouwman et al. deposit a series of lanthanoid MOF LnHL (Ln = Tb, Gd, and $Gd_{0.9}Tb_{0.1}$; H_4L = 5-hydroxy-1,2,4-benzenetricarboxylic acid) films on a Gd_2O_3 substrate [101]. As the temperature increases from 110 to 270 K, the intensity of the Tb^{III} -based emission in the $Gd_{0.9}Tb_{0.1}HL$ film only changes slightly, but the intensity of the ligand-based phosphorescence decreases dramatically. A good linear relationship is found based on the ratio between the intensities I_{Tb} (541 nm) and $I_{(phos+Tb)}$ (the total emission intensity from 350 to 650 nm). The relative sensitivity of $Gd_{0.9}Tb_{0.1}HL$ film is $0.8\% K^{-1}$, which can be enhanced with a lower Tb content and the relative sensitivity of $Gd_{0.99}Tb_{0.01}HL$ compound reaches up to $4.4\% K^{-1}$ at 110 K.

4.2. Ion Detection

With the development of modern industry, heavy metal ions, such as Cu^{2+} , Hg^{2+} , Cr^{3+} from industrial wastes, have increasingly released into the environment, which causes a series of ecological and health-care issues [102]. Wastewater containing high concentrations of Cu^{2+} will seriously pollute the soil and endanger the ecosystem of the natural water system. For human bodies, excessive intake of copper ion may cause gastrointestinal distress, liver and kidney failure, even DNA damage [91,103–106]. Hg^{2+} is among the most toxic metal ions, which is harmful to humans and can cause many diseases, such as digestive, kidney, and neurological diseases, even in a very low concentration. It is very difficult to be replaced in a short period of time when mercury enters the human body [107–114]. As for Cr^{3+} , a trace amount of Cr^{3+} is necessary and has a huge impact on the metabolism of carbohydrates, fats, proteins, and nucleic acids. The deficiency of Cr^{3+} can trigger diabetes, atherosclerosis, and cardiovascular diseases. However, excess Cr^{3+} is still toxic and harmful to human health, which can incorporate with DNA and result in mutations and malignant cells [115,116]. Besides, anions have important roles in a wide variety of environmental, industrial, biological and clinical fields. For example, the carbonate ion concentration in blood maintains an approximation of the acid-base balance and aids in elucidating abnormal conditions [77,117,118]. Therefore, it is urgently needed to develop simple, fast, visual techniques for detecting these ions.

4.2.1. Cu^{2+} Sensing

Several reports have manifested the potential applications of luminescent MOFs in the bio-sensing of Cu^{2+} ion. In 2010, Chen and Qian et al. reported a microporous luminescent MOF $Eu_2(FMA)_2(OX)(H_2O)_4 \cdot 4H_2O$ (FMA = fumarate; OX = oxalate) for the sensing of Cu^{2+} [103]. The luminescent intensity of $Eu_2(FMA)_2(OX)(H_2O)_4 \cdot 4H_2O$ largely quenches in the presence of Cu^{2+} , and the sensing ability under simulated physiological conditions is explored. Zhu et al. report a europium-based MOF probe with a high quenching coefficient of Cu^{2+} among reported MOFs [104]. The exchange of Cu^{2+} with the cationic guest molecule causes decomposition of the skeleton, resulting in quenching of the luminescent. Employing special chemical reaction is designed for specific Cu^{2+} probe by Oh et al. [105]. They synthesize a pyrene-functionalized organic building block CPP-16 with three functional parts: a framework construction part, a detecting part and a fluorophore part. The interaction of Cu^{2+} with amide groups results in change of the dangled pyrene groups from the stacked excimer state to the quenched excimer state, leading to significant quenching of the fluorescence.

Considering that the biosensing of Cu^{2+} ions is usually in the liquid phase, the portable MOF films can apparently make the detection procedure simpler. Yang et al. utilize the one-step electrodeposition method to fabricate a luminescent water stable Tb-Succinate MOF film on FTO conductive glass. The photoluminescence experiment suggests that the Tb-Succinate MOF film exhibits characteristic luminescence of Tb^{3+} ion, and presents high sensitive and selective sensing ability toward Cu^{2+} ion [91]. The quenching percentage of the luminescence can be linearly fit to the concentration of the Cu^{2+} ions with a K_{SV} value of $6298 M^{-1}$. As shown in Figure 16, the luminescent quenching effects are eye-distinguishable under UV-light when the concentration of Cu^{2+} ions is between 1×10^{-5} to 1×10^{-3} M. Compared with the powder sample, the Tb-Succinate MOF film not

only has brighter luminescence, but also exhibits faster luminescent response of Cu^{2+} in the first 10 min. The film provides potential for semi-quantitative in-field detection of Cu^{2+} ion in aqueous environments or biosystems. The same group also demonstrates the potential of luminescent Ln-CP film $\text{Tb}_2(\text{BDC})_3(\text{H}_2\text{O})_4$ for Cu^{2+} ions sensing [106].

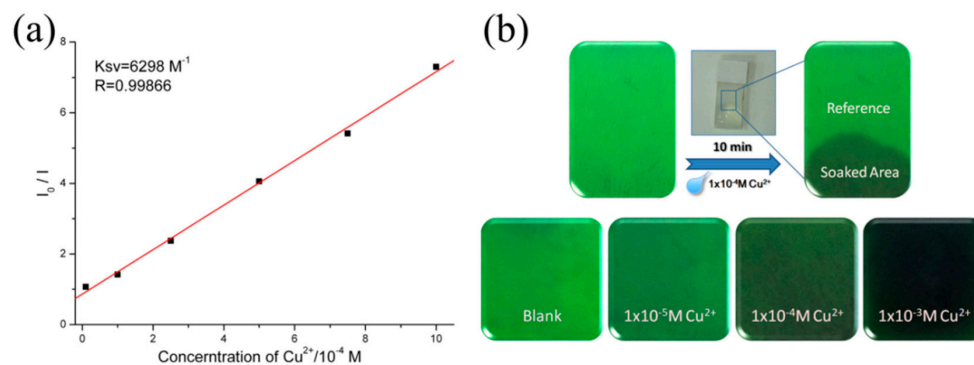


Figure 16. (a) Stern–Volmer plot of the Tb-Succinate MOF film sensing of Cu^{2+} at the range from 1×10^{-5} to 1×10^{-3} M. The line represents the linear fit of the data; (b) Photographs of the Tb-Succinate film before and after the addition of different Cu^{2+} solutions under UV-light radiation at a wavelength of 254 nm. Reprinted with permission from Reference [91]. Copyright 2015 Elsevier.

4.2.2. Hg^{2+} Sensing

The mercury ion (Hg^{2+}) has a higher affinity to nitrogen atoms and MOFs containing uncoordinated pyridyl nitrogen atoms are usually used to sense Hg^{2+} ions [107]. Yang et al. reported a robust MOF thin films $[\text{Eu}_2(\text{bqdc})_3(\text{H}_2\text{O})(\text{DMF})_3] \cdot 0.5\text{DMF} \cdot \text{H}_2\text{O}$ ($\text{bqdc} = 2,2'$ -biquinoline-4,4'-dicarboxylate) for Hg^{2+} ion sensing [108]. The film of $[\text{Eu}_2(\text{bqdc})_3(\text{H}_2\text{O})(\text{DMF})_3] \cdot 0.5\text{DMF} \cdot \text{H}_2\text{O}$ with a thickness of about 10 μm is developed by electrodeposition in combination with subsequent solvothermal synthesis (Figure 17). Due to the diffusion of Hg^{2+} into the channels and coordination with the pyridyl atom on bqdc^{2-} , the energy transfer from the antenna of bqdc^{2-} to Eu^{3+} is interfered, resulting in the quenching of the Eu^{3+} luminescence. This sensor can measure the concentration of Hg^{2+} in the range from 1×10^{-5} to 1×10^{-3} M with a detection limit of 1×10^{-8} M. Besides, the change in the photoluminescence intensity of this sensor before and after the exposure to Hg^{2+} is distinguishable even with the naked eye. In addition, the performance of film for Hg^{2+} sensing is superior to that of emulsion and powder in practicability and data reproducibility.

Some other nitrogen-containing groups are also incorporated into the MOFs for Hg^{2+} ion detection. By immobilizing melamine groups into the organic linker 4,4',4''-s-triazine-1,3,5-triyltri-*p*-aminobenzoic acid (H_3TATAB), Qian and Cui et al. synthesize a lanthanide MOF $\text{Tb}(\text{TATAB}) \cdot (\text{DMF})_4(\text{H}_2\text{O})(\text{MeOH})_{0.5}$ for Hg^{2+} sensing [109]. The suitable space between multiple nitrogen atoms from triazine and imino groups is beneficial for chelating with Hg^{2+} ions, and this sensor is successfully applied to detect Hg^{2+} ions in natural water samples. Gu et al. utilize a PCN-224 containing porphyrin ring to detect Hg^{2+} in the 4-(2-hydroxyethyl)-piperazine-1-ethanesulfonic acid (HEPES) buffer solution [110]. The Hg^{2+} ions bind to the porphyrin center, providing a fluorescent quenching effect in the visible region. The fluorescence quenching shows a linear correlation in the Hg^{2+} concentration range from 0.1 to 10 μM with the calculated limit of detection (LOD) of 6 nM. In addition, amino [111], triazole unit [112], sulfone [113] and thiol [114] are introduced into MOFs for Hg^{2+} sensing.

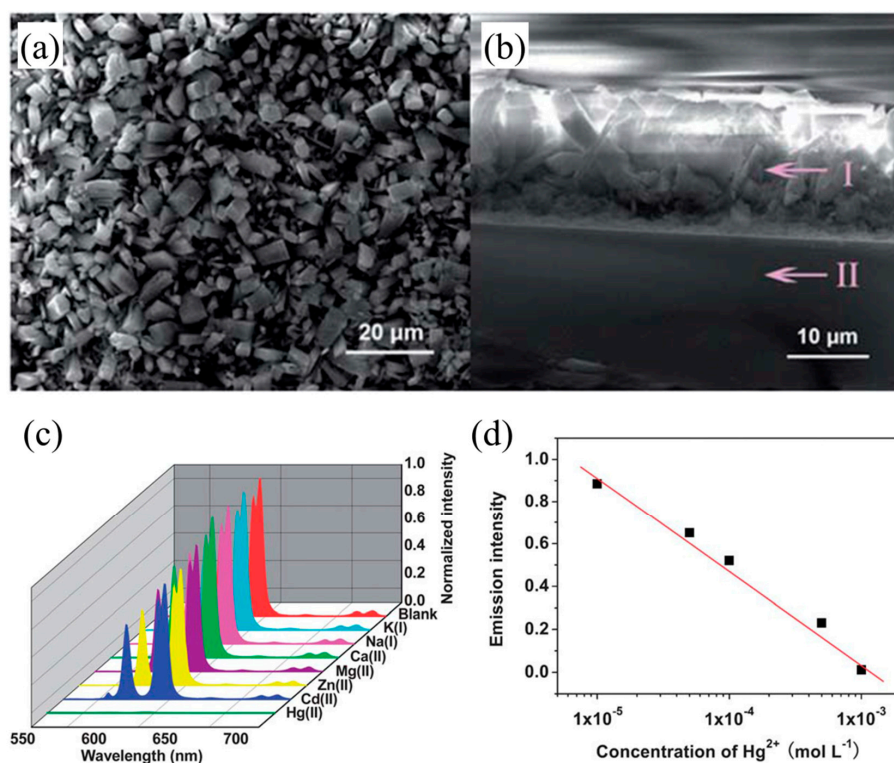


Figure 17. SEM images of a film $[\text{Eu}_2(\text{bqdc})_3(\text{H}_2\text{O})(\text{DMF})_3] \cdot 0.5\text{DMF} \cdot \text{H}_2\text{O}$: (a) top view and (b) cross-sectional view (I = $[\text{Eu}_2(\text{bqdc})_3(\text{H}_2\text{O})(\text{DMF})_3] \cdot 0.5\text{DMF} \cdot \text{H}_2\text{O}$, II = ITO glass); (c) Emission spectra of the film of $[\text{Eu}_2(\text{bqdc})_3(\text{H}_2\text{O})(\text{DMF})_3] \cdot 0.5\text{DMF} \cdot \text{H}_2\text{O}$ after being immersed in various metal ions at 1×10^{-3} M; (d) Emission intensities of the film of $[\text{Eu}_2(\text{bqdc})_3(\text{H}_2\text{O})(\text{DMF})_3] \cdot 0.5\text{DMF} \cdot \text{H}_2\text{O}$ immersed in Hg^{2+} at various concentrations. Reprinted with permission from Reference [108]. Copyright 2013 the Royal Society of Chemistry (London, UK).

4.2.3. Cr^{3+} Sensing

Cao et al. demonstrate the potential of Ln-BTC MOFs films to detect chromium ions (Cr^{3+}) [115]. First, dense and continuous Tb-BTC, Eu-BTC and $\text{Eu}_{0.45}\text{Tb}_{0.55}$ -BTC MOF films are fabricated directly on the unmodified zinc, FTO and ITO-substrates by the electrophoretic deposition method. The thicknesses of these three films are 55, 67, and 33.5 μm , respectively, and the film thickness can be controlled by the DC voltage. When excited with UV light at 254 nm, Tb-BTC, Eu-BTC, and $\text{Eu}_{0.45}\text{Tb}_{0.55}$ -BTC films exhibit strong green, red, and yellow luminescence, respectively. Then, the prepared Tb-BTC film is used to detect Cr^{3+} . Fluorescence titration experiments show that the Tb-BTC film could successfully detect Cr^{3+} at a concentration of 10^{-4} mM (0.11 ppb) with the fast response time of 10 s. In another case, Zhang et al. synthesize a stable fluorescent framework $[\text{Me}_2\text{NH}_2]_4[\text{Zn}_6(\text{qptc})_3(\text{trz})_4] \cdot 6\text{H}_2\text{O}$ (H_4qptc = terphenyl-2,5,2'5'-tetracarboxylic acid, trz = 1,2,4-triazole), which exhibits selective adsorption and recyclable detection of the Cr^{3+} ion with $K_{\text{SV}} = 4.39 \times 10^4 \text{ M}^{-1}$ [116].

4.2.4. CO_3^{2-} Sensing

Yang et al. fabricate a luminescent Ln-MOF-based thin film $[\text{Eu}(\text{HBPTC})(\text{H}_2\text{O})_2] \cdot 2\text{DMF}$ (BPTC = benzophenone-3,3',4,4'-tetracarboxylic) via electrodeposition for the detection of CO_3^{2-} [77]. The thin films of Eu-HBPTC are deposited at the cathode trough by a mechanism of electrochemical generation of the base in a nitrate solution. As shown in Figure 18a, the reduction of NO_3^- causes the local increase of HO^- concentration, followed by the hydrolysis of benzophenone-3,3',4,4'-tetracarboxylic dianhydride (BTDA) and the consequent growth of MOFs directly on the FTO surface. Upon the excitation

at 317 nm, the Eu-HBPTC film exhibits the characteristic emission of Eu^{3+} ions. The emission intensity can be exclusively quenched by CO_3^{2-} (Figure 18b), which might be attributed to the impediment of the energy transfer between the linkers and Eu^{3+} ions. In a recent work, Yan et al. present a robust and porous Eu/Pt-MOF for the ratiometric sensing towards CO_3^{2-} . With the increase of CO_3^{2-} , the luminescence of Eu^{3+} is enhanced while the ligand emission is suppressed significantly [117]. The intensity ratio of two emissions linearly increases as the concentration of CO_3^{2-} with a detection limit of $0.021 \mu\text{M}$ increases. The same group further establishes an orthogonal pattern based on luminescent intensity and quantum yields of MIL-125(Ti)-AM-Eu in response to various anions [118]. The ratiometric luminescence and the quantum yields of the MOF show a one-to-one correspondence with the accommodated anions, which provides a simple identification method to recognize different anions by reading the coordinates on the pattern.

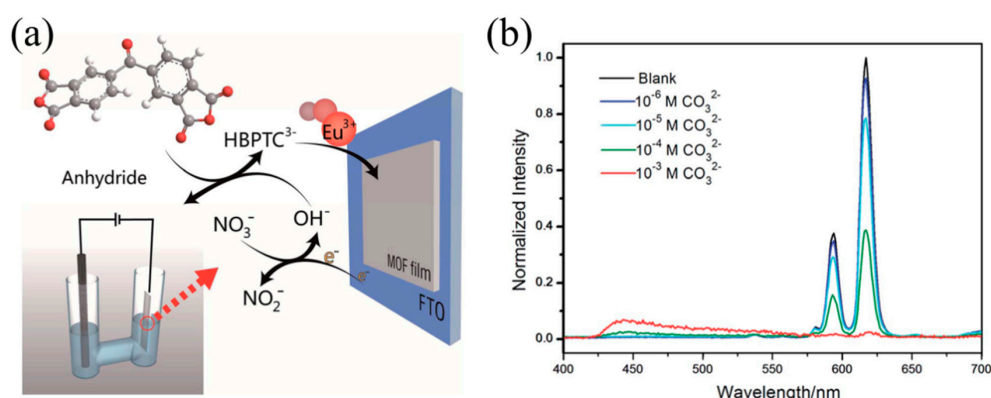


Figure 18. (a) General scheme for the cathodically induced electrodeposition of MOFs, involving the reduction in nitrate and generation of HO^- , the hydrolysis of anhydride (BTDA) and, MOF crystallization from HBPTC^{3-} and Eu^{3+} ; (b) Emission spectra of the MOF film after being immersed in an aqueous CO_3^{2-} solution at various concentrations (excited at 317 nm). Reprinted with permission from Reference [77]. Copyright 2014 the Royal Society of Chemistry (London, UK).

4.3. Gas Detection

Compared with the luminescent sensors in the form of powders and suspensions, film-based probes have significant advantages in gas detection. The dispersion of MOF powders into solutions is time-consuming, and the powdery samples and suspensions are hard to be recycled. In addition, the powdery samples cannot stand the blast of gas flux. Therefore, luminescent MOF film-based probe is a good choice for gas detection.

Qian and Cui et al. recently reported two indium MOF films, $[(\text{CH}_3)_2\text{NH}_2][\text{In}_3\text{O}(\text{BTC})_2(\text{H}_2\text{O})_3]_2[\text{In}_3(\text{BTC})_4]$ (CPM-5) and $\text{In}_3\text{O}(\text{OH})(\text{H}_2\text{O})_2[\text{BTC}]_2$ (MIL-100(In)), for oxygen sensing [94,119]. The CPM-5 and MIL-100(In) films are prepared by the in situ solvothermal synthesis method on ITO glass with the “twin indium source” strategy, and Tb^{3+} ions are introduced into these two films through the post-functionalization. As shown in Figure 19, the prepared films are continuous and dense with the thickness of about $2.5 \mu\text{m}$, and the modifications barely change the structures and the morphology of the MOF films.

Both CPM-5 $\supset \text{Tb}^{3+}$ and MIL-100(In) $\supset \text{Tb}^{3+}$ thin films exhibit the characteristic emission bands of Tb^{3+} , and the luminescence of these films can be gradually quenched by the increasing pressure of O_2 (Figure 20b). Although the lanthanide ions are sensitized by the same organic ligand, the quenching efficiencies of CPM-5 $\supset \text{Tb}^{3+}$ and MIL-100(In) $\supset \text{Tb}^{3+}$ films are about 47% and 88% at 1 atm of O_2 , respectively. It might be because of different energy transfers in these two films. In CPM-5 $\supset \text{Tb}^{3+}$, Tb^{3+} ions serve as balancing cations in the pores, leading to long-distance intermolecular energy transfer, while MIL-100(In) possesses exposed carboxylate acids to form Tb-O bonds with metal ions,

leading to the intramolecular energy transfer (see Figure 20a). As a result, the MIL-100(In) \Rightarrow Tb³⁺ film shows higher oxygen sensitivity ($K_{SV} = 7.59$) and shorter response/recovery time (6 and 53 s) than those of CPM-5 \Rightarrow Tb³⁺ film (see Figure 20c,d).

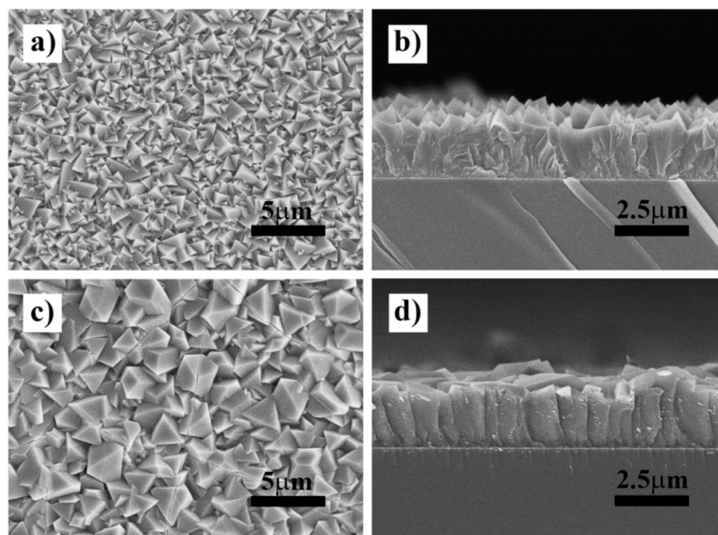


Figure 19. SEM images of CPM-5 \Rightarrow Tb³⁺ (a,b) and MIL-100(In) \Rightarrow Tb³⁺ (c,d) films. Reprinted with permission from Reference [94]. Copyright 2014 the American Chemical Society (Washington, DC, USA).

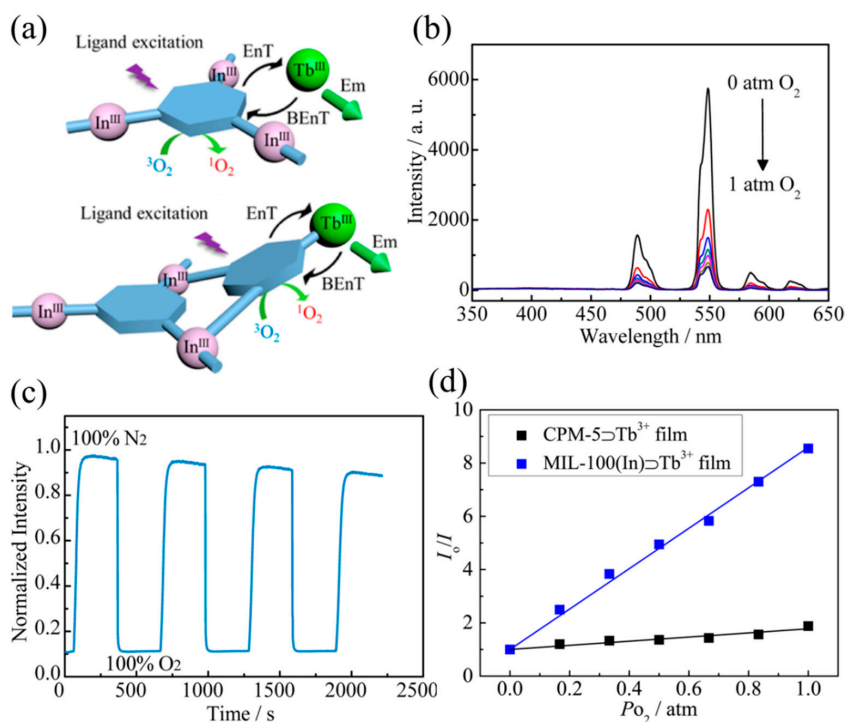


Figure 20. (a) Energy transfer process and O₂ quenching process of CPM-5 \Rightarrow Tb³⁺ (upper) and MIL-100(In) \Rightarrow Tb³⁺ (lower); (b) Emission spectra of activated MIL-100(In) \Rightarrow Tb³⁺ films under different oxygen partial pressures P_{O_2} ; (c) Reversible luminescence quenching of the MIL-100(In) \Rightarrow Tb³⁺ film upon alternating exposure to 1 atm of O₂ and N₂; (d) Stern–Volmer plots showing I_0/I vs oxygen partial pressure P_{O_2} for the two activated MOF films. Reprinted with permission from Reference [94]. Copyright 2014 the American Chemical Society (Washington, DC, USA).

By introducing the Pt(II)-porphyrin ligand into the frameworks, Lin's group report the first self-calibrating oxygen probe to be utilized in living cells [120]. Two different linkers with a similar length, named H₂DBP-Pt (DBP-Pt = Pt-5,15-di(p-benzoato)porphyrin) and H₂QPDC-NH₂, (H₂QPDC-NH₂ = amino-quaterphenyldicarboxylic acid), are successfully introduced into one NMOF. Then, Rhodamine-B isothiocyanate (RITC) is conjugated in QPDC-NH₂ linkers via thiourea bonds. The DBP-Pt ligand acts as an O₂-sensitive probe and a Rhodamine-B isothiocyanate ligand acts as an O₂-insensitive reference probe. The modified NMOF shows a linear correlation between the intensity ratio and P_{O2} and is further used to probe oxygen in living cells.

MOF film-based probes for other gases, such as ammonia, sulfur dioxide, nitrobenzene (NB) and trinitrotoluene (TNT) in gas phases, and gaseous HCl, have been explored. Qian and Cui et al. prepare an MIL-124 film by the in situ synthesis method on a porous α -Al₂O₃ ceramic plate, and introduce europium ions into the film via post-synthetic modification [95]. The luminescent MOF film MIL-124@Eu³⁺ can detect ammonia based on the chemical reaction between NH₃ and the free -COOH in the framework. The same group recently reported a Eu-BDC-NH₂ film for detecting sulfur dioxide with a detection limit of 0.65 ppm [62]. Yang et al. design an electrodeposited luminescent MOF thin film [Eu₂(TDC)₃(CH₃OH)₂].CH₃OH (Eu-TDC, TDC = thiophene-2,5-dicarboxylate) for detecting nitrobenzene vapor [121]. Cao et al. synthesize a Tb-BTC film to detect NB and TNT in the gas phase [115]. Dong et al. report a porous Cu₄I₄-MOF-based MMM for visual and luminescent detection of gaseous HCl [122].

4.4. Biomolecule Detection

4.4.1. Formaldehyde

Formaldehyde (HCHO) is widely used in construction, and furniture, particleboard and other industries. However, it is very harmful to human being and can result in watery eyes, asthma and respiratory irritation. However, some unscrupulous vendors, driven by economic interests, often add HCHO to the soaking solution to extend the keeping life of waterlogged food products. Therefore, it is necessary to monitor them in light of their importance not only as air pollutants but also as indicators of food quality. Yang et al. recently designed a luminescent thin film of Eu-NDC@HPAN for self-calibrating formaldehyde sensing [123]. The Eu-NDC@HPAN film is fabricated on polyacrylonitrile (PAN) via a layer by the layer strategy (see Figure 21). A hydrolyzed polyacrylonitrile (HPAN) film is immersed in a Eu(NO₃)₃·6H₂O solution, causing the binding of Eu³⁺ ions to -COO on the surface of HPAN. After removing unreacted Eu³⁺ ions, the HPAN film is put into the NDC solution to make the binding between Eu³⁺ and NDC. By subsequently repeating and alternating the immersion of HPAN film in the solution of Eu(NO₃)₃·6H₂O and NDC, square Eu-NDC particles with the size of 2–4 μ m grow on the surface of HPAN homogeneously (see Figure 22a,b).

Upon excitation at 360 nm, the Eu-NDC@HPAN film exhibits characteristic emission of the Eu³⁺ ion. When exposed to HCHO, the luminescence intensity of the emission at 616 nm is significantly quenched, while luminescence intensity of the emission at 453 nm becomes conspicuous, but other small molecules (propanol, acetone, DMF, H₂O MeOH, and EtOH) show weak influence (see Figure 22c). There is a linear relationship between the emission ratios (I_{453}/I_{616}) and the concentrations of HCHO from 0.05 to 1% (see Figure 22d). The Eu-NDC@HPAN film is further used to detect HCHO in an aquatic product and an HCHO vapor. These results suggest that the Eu-NDC@HPAN can be potentially applied in practical applications for the quantitative determination of HCHO.

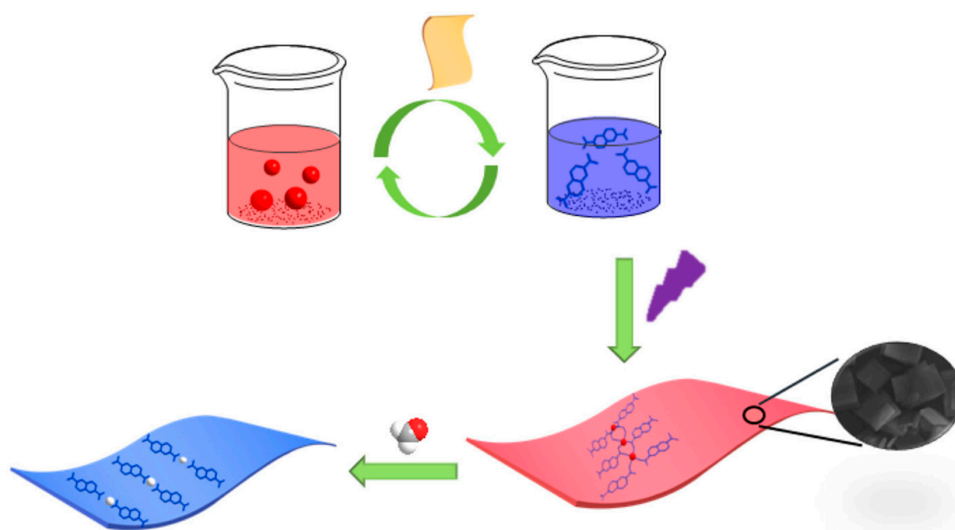


Figure 21. Schematic representation of the synthesis process of Eu-NDC@HPAN and the luminescence quenching phenomenon of HCHO to Eu-NDC@HPAN. Reprinted with permission from Reference [123]. Copyright 2017 Elsevier.

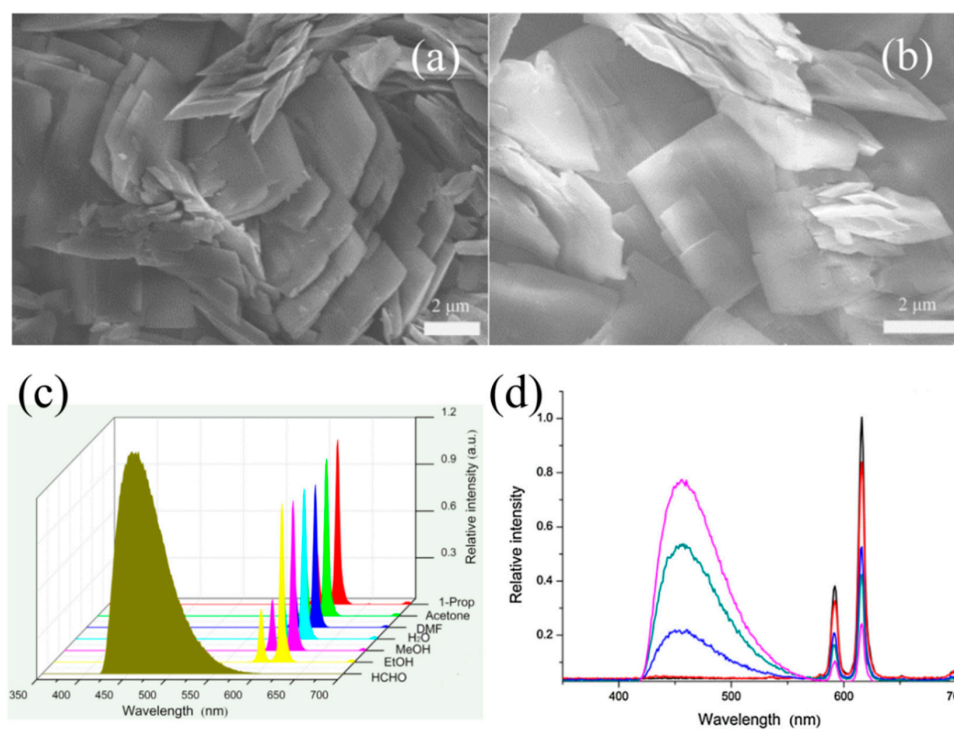


Figure 22. SEM images of Eu-NDC@HPAN: (a) top view and (b) enlarged view of (a); (c) Luminescence spectra of Eu-NDC@HPAN treated with different small molecules; (d) Luminescence spectra of Eu-NDC@HPAN as a function of the formaldehyde concentrations (from top to bottom: 1, 0.5, 0.25, 0.1, 0.05%) in aqueous solutions. Reprinted with permission from Reference [123]. Copyright 2017 Elsevier.

4.4.2. Pharmaceuticals

The recognition and detection of pharmaceuticals are important in biological and environmental systems. Wang et al. recently reported a luminescent mixed-crystal Ln-MOF thin film, $\text{Eu}_x\text{Tb}_{1-x}\text{-BTC}$, for the sensing of pharmaceuticals [92]. The nanocrystals $\text{Eu}_x\text{Tb}_{1-x}\text{-BTC}$ is first synthesized with sodium acetate as a modulator. Then, the monodisperse nanocrystals are dip-coated on ITO glass to obtain the

large-scale, uniform and continuous thin film with a thickness of 4–5 μm (Figure 23a,b). Prepared films exhibit the characteristic transitions of Eu^{3+} and Tb^{3+} , and different pH conditions (4–9) and different solutions (pure water, river water, saline and simulated body fluid) have little effect on the emissions. However, due to the different host–guest interactions, the emission intensity of $\text{Eu}_{0.1}\text{Tb}_{0.9}$ -BTC film is largely dependent on the pharmaceutical molecules, such as antipyrine, benzafibrate, caffeine, clofibrate, clotetracycline, coumarin, diclofenac, fluorouracil, nalidixic acid, naproxen, sulfachinoxalin, and tetracycline. The parameter $(R - R_0)/R_0$ is used to fingerprint correlations between each different pharmaceutical molecule, where R_0 is the initial intensity ratio without an analyte and R is the intensity ratio in the presence of an analyte (Figure 23c). Moreover, the $\text{Eu}_{0.1}\text{Tb}_{0.9}$ -BTC film emits different guest-dependent light colors, which can be distinguished by the naked eye (Figure 23d).

Coumarin and caffeine are selected as target compounds to investigate the quantitative relationship between the concentration and intensity ratio of $\text{Eu}_{0.1}\text{Tb}_{0.9}$ -BTC. As the concentration increases, the $(R - R_0)/R_0$ of coumarin increases linearly with a slope of about 0.0276 ± 0.0006 , while the $(R - R_0)/R_0$ of caffeine decreases linearly with a slope of -0.0045 ± 0.002 . The values of $(R - R_0)/R_0$ obtained from simulated samples are basically consistent with the detection curves, indicating that the $\text{Eu}_{0.1}\text{Tb}_{0.9}$ -BTC film is a luminescent sensor candidate in practical applications.

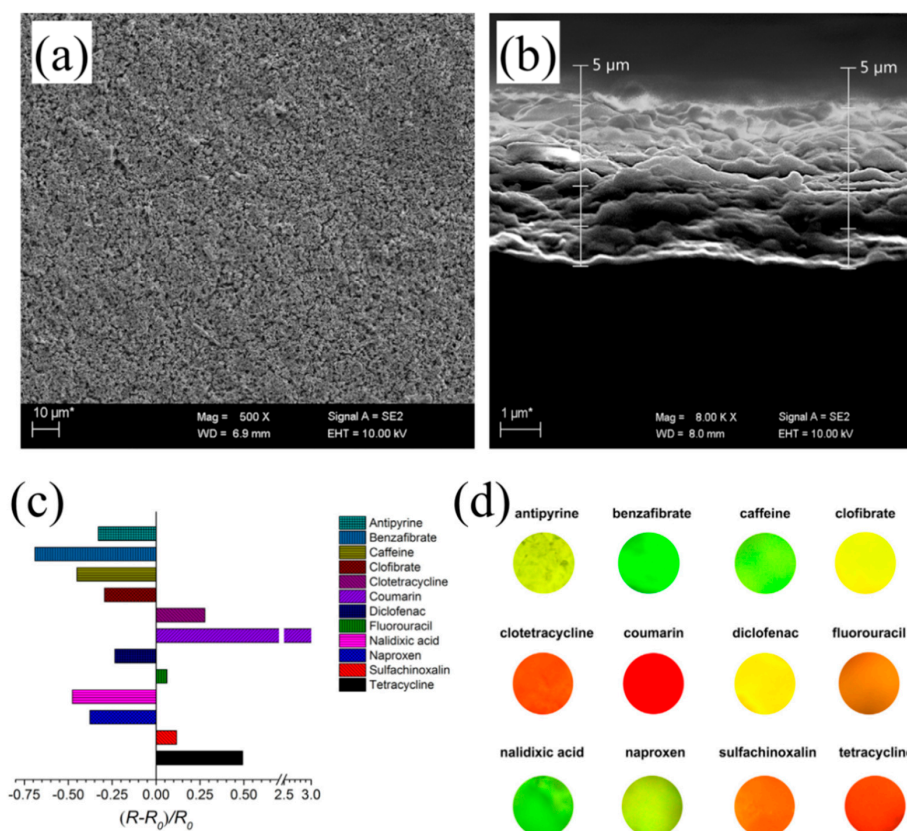


Figure 23. SEM images of (a) the surface and (b) the cross section of $\text{Eu}_{0.1}\text{Tb}_{0.9}$ -BTC film; The emission intensity ratio changes (c) and the optical photographs (d) of $\text{Eu}_{0.1}\text{Tb}_{0.9}$ -BTC thin film in the presence of different analytes (20 mL, 10^{-4} M). Reprinted with permission from Reference [92]. Copyright 2018 Elsevier.

4.4.3. Nitrofurantoin Antibiotics

Nitrofurantoin antibiotics (NFAs) have effective therapeutic value for the treatment of protozoan and bacterial infections in human and prevent the infection of intestinal tract bacteria in food-producing animals. However, due to the mutagenicity and carcinogenicity, NFAs have been banned in the United

States, China, and most other countries. Development of rapid and effective methods for the detection of NFAs is very necessary on ecosystem and human health. Recently, Yang et al. fabricated two MOF films $[\text{Eu}_2(\text{BCA})_3(\text{H}_2\text{O})(\text{DMF})_3] \cdot 0.5\text{DMF} \cdot \text{H}_2\text{O}$ (Eu-BCA, BCA = 2,2'-biquinoline-4,4'-dicarboxylate) and $[\text{Tb}_2(\text{AIP})_2(\text{H}_2\text{O})_{10}] \cdot (\text{AIP}) \cdot 4\text{H}_2\text{O}$ (Tb-AIP, AIP = 5-aminoisophthalate) for NFA detection [124,125].

The Eu-BCA film is coated by vertically inserting the Co_3O_4 nanowire-coated stainless steel wire mesh (SSWM) into the MOF precursor solution [124]. When the bare SSWM is used directly, the film cannot be formed on the SSWM. These Co_3O_4 motifs act as anchors and nucleation centers to fix the MOF crystals on every stainless steel wire firmly. The concentration of MOF precursor solution has a significant influence on the resulting films. Relatively low concentrations of precursor solution (0.005 M and 0.01 M) lead to some scattered MOF crystal blocks piled up on the modified SSWM. With the increasing concentrations to 0.015 M and 0.02 M, a continuous and compact Eu-BCA thin-film is formed on the substrate (Figure 24).

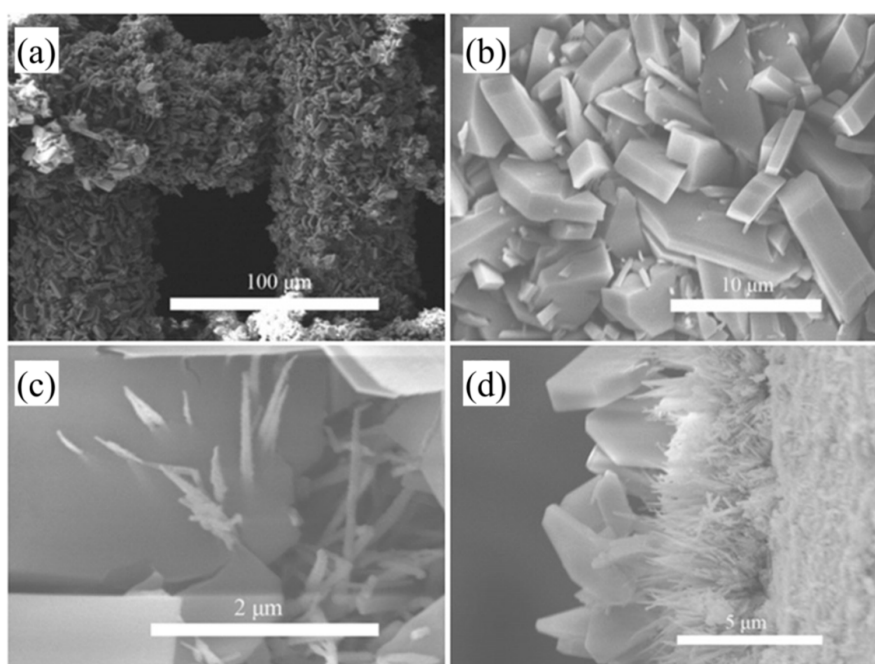


Figure 24. (a,b) SEM images of Eu-BCA thin-films on the stainless steel wire mesh (SSWM); (c) SEM image of Co_3O_4 nanowire array-threaded Eu-BCA MOF crystal plates; (d) cross-sectional image of Eu-BCA thin films. Reprinted with permission from Reference [124]. Copyright 2017 WILEY-VCH Verlag GmbH & Co., (Weinheim, Germany).

The Eu-BCA film exhibits the characteristic emission of Eu^{3+} when excited with UV light, which is dramatically quenched by nitrofurans antibiotics nitrofurazone (NFZ) and nitrofurantoin (NFT). The K_{sv} value are $2.2 \times 10^{-4} \text{ M}^{-1}$ for NFZ and $1.6 \times 10^{-4} \text{ M}^{-1}$ for NFT. The corresponding limits of detection for NFZ and NFT are estimated to be 0.21 and 0.16 μM , respectively. The Eu-BCA film can selectively detect NFAs even in the presence of a high concentration of other antibiotics, such as metronidazole (MDZ), dimetridazole (DTZ), sulfadiazine (SDZ), sulfamethazine (SMZ), chloramphenicol (CAP), thiamphenicol (THI), and penicillin (PCL) (Figure 25). Further, this thin film can detect NFAs in real samples, and can also be recycled.

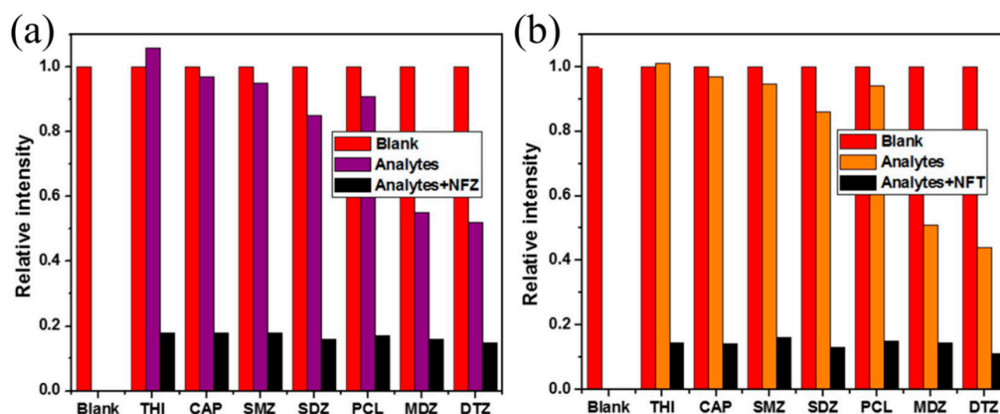


Figure 25. Fluorescent response of the Eu-BCA thin-film towards other competing antibiotics (1.0 mM) or a mixture of competing antibiotics (1.0 mM) and nitrofurazone (NFZ) and (b) for nitrofurantoin (NFT). Reprinted with permission from Reference [124]. Copyright 2017 WILEY-VCH Verlag GmbH & Co., (Weinheim, Germany).

The Tb-AIP film is fabricated by the MMM method with poly(methyl methacrylate) (PMMA) as the polymer and Tb-AIP as the fillers (Figure 26) [125]. Tb-AIP MOF powder fillers are added to the PMMA chloroform solution and then ultrasonically dispersed in ice water for 30 min to get PMMA-MOF ink. The luminescent MMMs are formed by dropping the above ink on slide glasses, followed by drying in an oven overnight. The freestanding luminescent sensor is obtained by peeling off the MMMs from slide glass.

Upon excitation at 360 nm, the emission spectrum of Tb-AIP MMMs exhibits four characteristic transitions of the Tb³⁺ ions. Tb-AIP MMMs can selectively and sensitively detect NFZ and NFT via the inner filter effect (IFE). Other common antibiotics, metal ions and anions have little interference with the detective results. The limits of detection for NFT and NFZ are 0.30 and 0.35 μM , respectively.

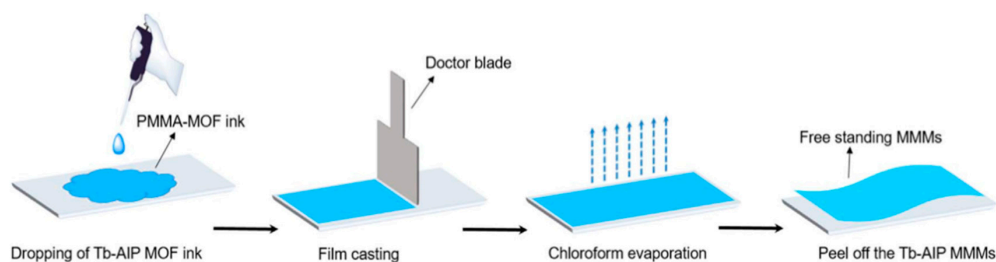


Figure 26. Schematic illustration for the preparation of Tb-AIP MMMs. Reprinted with permission from Reference [125]. Copyright 2017 WILEY-VCH Verlag GmbH & Co., (Weinheim, Germany).

5. Conclusions and Outlook

Based on the above discussion, it is obvious that luminescent MOF thin films have received tremendous attention in a wider range of applications in biosensing. Various methods of assembling the luminescent MOF thin films are the foundation of these achievements. However, deposited films from solvothermal mother solutions are out of universality and the obtained films are often discontinuous. Preparing highly oriented single crystal and polycrystalline MOF films remains a significant challenge. Owing to the facile operation and general applicability, the electrochemical synthesis and drop-casting method are increasingly employed. However, they suffer from some inborn weaknesses including poor uniformity and adhesion, and their sensing performances are significantly influenced by the film thickness. In addition, in the MMMs, the MOF particles are encapsulated by the

organic polymer and cannot sufficiently interact with the analytes, which loses the porosity of MOFs and leads to poor sensitivity.

The development of luminescent MOF film-based biosensors yields significant advancements in environmental monitoring, and biomedical diagnostics. However, the study of luminescent MOF film-based biosensors is a relatively new field and more research work is needed. Current challenges in the application of luminescent MOF films as biosensors include reversible binding to analytes, which would realize continuous detection. To achieve this goal, advanced structural design based on a thorough investigation of the structure–property relationship of MOFs is required. The fluorescent efficiency of MOFs still restrains the LOD in biomedical sensing fields, and development of more efficient luminescent MOF films can further increase the detection limit. In addition, most of the MOF film sensors are based on the intensity change of single emission, which is greatly affected by the concentration of probe, excitation power, and the drifts of the optoelectronic system. The strategy utilizing the ratio between the intensities of two transitions of the same probe has been established and thus opened a new strategy for high-accuracy luminescent sensors. Moreover, the development of a new multi-dimensional sensing strategy utilizing intensity, life, wavelength, and polarization could be an attractive future direction for improving sensor accuracy.

There are numerous essential metals (e.g., Cr, Mn, Co, Ni, Mo) and toxic metals (e.g., Cd, Hg, Pb) to be detected and monitored in the biomedical field. In this regard, development of new MOF sensors will be attractive in the future. Research on biomedical sensing applications of MOF thin films is gaining momentum and this emerging new class of materials is likely to replace the traditional film materials in the future. Systematic investigations concerning critical issues, such as the stability of MOFs under humid environment and toxicology, will be necessary and speed up the development of luminescent MOF films. Besides, further efforts should focus on the preparation of biologically compatible luminescent MOF films and the integration of different functions, such as luminescence sensing, imaging, molecular targeting, and so on. More research effort is needed to prepare MOF films that meet different testing requirements, and there is still a long way to go before these materials can be industrialized and commercialized.

Author Contributions: Writing of the original draft preparation, Z.L. and T.X.; writing of review and editing, E.Y. and Y.C.

Funding: This work was supported by the National Natural Science Foundation of China (No. 81771158), the Science Foundation from Health Commission of Zhejiang Province (No.ZKJ-ZJ-1503, 2016147373, 2017ZA005), and the Zhejiang medical innovation discipline (Rehabilitation of Neurology).

Conflicts of Interest: The authors declare no conflicts of interest.

References

1. Kirsch, J.; Siltanen, C.; Zhou, Q.; Revzin, A.; Simonian, A. Biosensor technology: Recent advances in threat agent detection and medicine. *Chem. Soc. Rev.* **2013**, *42*, 8733–8768. [[CrossRef](#)] [[PubMed](#)]
2. Turner, A.P.F. Biosensors: Sense and sensibility. *Chem. Soc. Rev.* **2013**, *42*, 3184–3196. [[CrossRef](#)] [[PubMed](#)]
3. Wang, X.-D.; Wolfbeis, O.S.; Meier, R.J. Luminescent probes and sensors for temperature. *Chem. Soc. Rev.* **2013**, *42*, 7834–7869. [[CrossRef](#)] [[PubMed](#)]
4. Wang, H.-S. Metal–organic frameworks for biosensing and bioimaging applications. *Coord. Chem. Rev.* **2017**, *349*, 139–155. [[CrossRef](#)]
5. Pramanik, S.; Zheng, C.; Zhang, X.; Emge, T.J.; Li, J. New Microporous Metal–Organic Framework Demonstrating Unique Selectivity for Detection of High Explosives and Aromatic Compounds. *J. Am. Chem. Soc.* **2011**, *133*, 4153–4155. [[CrossRef](#)] [[PubMed](#)]
6. Zhang, K.; Zhou, H.; Mei, Q.; Wang, S.; Guan, G.; Liu, R.; Zhang, J.; Zhang, Z. Instant visual detection of trinitrotoluene particulates on various surfaces by ratiometric fluorescence of dual-emission quantum dots hybrid. *J. Am. Chem. Soc.* **2011**, *133*, 8424–8427. [[CrossRef](#)] [[PubMed](#)]
7. You, L.; Zha, D.; Anslyn, E.V. Recent advances in supramolecular analytical chemistry using optical sensing. *Chem. Rev.* **2015**, *115*, 7840–7892. [[CrossRef](#)] [[PubMed](#)]

8. Shanmugaraju, S.; Mukherjee, P.S. π -Electron rich small molecule sensors for the recognition of nitroaromatics. *Chem. Commun.* **2015**, *51*, 16014–16032. [[CrossRef](#)] [[PubMed](#)]
9. Ding, S.-Y.; Dong, M.; Wang, Y.-W.; Chen, Y.-T.; Wang, H.-Z.; Su, C.-Y.; Wang, W. Thioether-Based Fluorescent Covalent Organic Framework for Selective Detection and Facile Removal of Mercury(II). *J. Am. Chem. Soc.* **2016**, *138*, 3031–3037. [[CrossRef](#)] [[PubMed](#)]
10. Shi, W.; Li, X.; Ma, H. A tunable ratiometric pH sensor based on carbon nanodots for the quantitative measurement of the intracellular pH of whole cells. *Angew. Chem. Int. Ed.* **2012**, *124*, 6538–6541. [[CrossRef](#)]
11. Feng, J.; Tian, K.; Hu, D.; Wang, S.; Li, S.; Zeng, Y.; Li, Y.; Yang, G. A Triarylboron-Based Fluorescent Thermometer: Sensitive Over a Wide Temperature Range. *Angew. Chem. Int. Ed.* **2011**, *50*, 8072–8076. [[CrossRef](#)] [[PubMed](#)]
12. Chen, Z.; Zhang, K.Y.; Tong, X.; Liu, Y.; Hu, C.; Liu, S.; Yu, Q.; Zhao, Q.; Huang, W. Phosphorescent Polymeric Thermometers for In Vitro and In Vivo Temperature Sensing with Minimized Background Interference. *Adv. Funct. Mater.* **2016**, *46*, 4386–4396. [[CrossRef](#)]
13. Miyata, K.; Konno, Y.; Nakanishi, T.; Kobayashi, A.; Kato, M.; Fushimi, K.; Hasegawa, Y. Chameleon Luminophore for Sensing Temperatures: Control of Metal-to-Metal and Energy Back Transfer in Lanthanide Coordination Polymers. *Angew. Chem. Int. Ed.* **2013**, *52*, 6413–6416. [[CrossRef](#)] [[PubMed](#)]
14. Kalytchuk, S.; Polakova, K.; Wang, Y.; Froning, J.P.; Cepe, K.; Rogach, A.L.; Zboril, R. Carbon Dot Nanothermometry: Intracellular Photoluminescence Lifetime Thermal Sensing. *ACS Nano* **2017**, *11*, 1432–1442. [[CrossRef](#)] [[PubMed](#)]
15. Guan, W.; Zhou, W.; Lu, J.; Lu, C. Luminescent films for chemo- and biosensing. *Chem. Soc. Rev.* **2015**, *44*, 6981–7009. [[CrossRef](#)] [[PubMed](#)]
16. Liu, J.; Sun, F.; Zhang, F.; Wang, Z.; Zhang, R.; Wang, C.; Qiu, S. In situ growth of continuous thin metal–organic framework film for capacitive humidity sensing. *J. Mater. Chem.* **2011**, *21*, 3775–3778. [[CrossRef](#)]
17. Stassen, I.; Burtch, N.; Talin, A.; Falcaro, P.; Allendorf, M.; Ameloot, R. An updated roadmap for the integration of metal–organic frameworks with electronic devices and chemical sensors. *Chem. Soc. Rev.* **2017**, *46*, 3185–3241. [[CrossRef](#)] [[PubMed](#)]
18. Cui, Y.; Song, R.; Yu, J.; Liu, M.; Wang, Z.; Wu, C.; Yang, Y.; Wang, Z.; Chen, B.; Qian, G. Dual-Emitting MOF \cap Dye Composite for Ratiometric Temperature Sensing. *Adv. Mater.* **2015**, *27*, 1420–1425. [[CrossRef](#)] [[PubMed](#)]
19. Miller, S.E.; Teplensky, M.H.; Moghadam, P.Z.; Fairen-Jimenez, D. Metal–organic frameworks as biosensors for luminescence-based detection and imaging. *Interface Focus* **2016**, *6*, 20160027. [[CrossRef](#)] [[PubMed](#)]
20. Xu, X.Y.; Lian, X.; Hao, J.N.; Zhang, C.; Yan, B. A Double-Stimuli-Responsive Fluorescent Center for Monitoring of Food Spoilage based on Dye Covalently Modified EuMOFs: From Sensory Hydrogels to Logic Devices. *Adv. Mater.* **2017**, *29*, 1702298. [[CrossRef](#)] [[PubMed](#)]
21. Lin, R.-B.; Li, F.; Liu, S.-Y.; Qi, X.-L.; Zhang, J.-P.; Chen, X.-M. A Noble-Metal-Free Porous Coordination Framework with Exceptional Sensing Efficiency for Oxygen. *Angew. Chem. Int. Ed.* **2013**, *52*, 13429–13433. [[CrossRef](#)] [[PubMed](#)]
22. Nagarkar, S.S.; Joarder, B.; Chaudhari, A.K.; Mukherjee, S.; Ghosh, S.K. Highly Selective Detection of Nitro Explosives by a Luminescent Metal–Organic Framework. *Angew. Chem. Int. Ed.* **2013**, *52*, 2881–2885. [[CrossRef](#)] [[PubMed](#)]
23. Hu, Z.; Deibert, B.J.; Li, J. Luminescent metal–organic frameworks for chemical sensing and explosive detection. *Chem. Soc. Rev.* **2014**, *43*, 5815–5840. [[CrossRef](#)] [[PubMed](#)]
24. Wang, B.; Lv, X.-L.; Feng, D.; Xie, L.-H.; Zhang, J.; Li, M.; Xie, Y.; Li, J.-R.; Zhou, H.-C. Highly Stable Zr(IV)-Based Metal–Organic Frameworks for the Detection and Removal of Antibiotics and Organic Explosives in Water. *J. Am. Chem. Soc.* **2016**, *138*, 6204–6216. [[CrossRef](#)] [[PubMed](#)]
25. Xia, T.; Zhu, F.; Cui, Y.; Yang, Y.; Wang, Z.; Qian, G. Highly selective luminescent sensing of picric acid based on a water-stable europium metal–organic framework. *J. Solid State Chem.* **2017**, *245*, 127–131. [[CrossRef](#)]
26. Zhang, L.-N.; Liu, A.-L.; Liu, Y.-X.; Shen, J.-X.; Du, C.-X.; Hou, H.-W. A luminescent europium metal–organic framework with free phenanthroline sites for highly selective and sensitive sensing of Cu²⁺ in aqueous solution. *Inorg. Chem. Commun.* **2015**, *56*, 137–140. [[CrossRef](#)]
27. Xu, X.-Y.; Yan, B. Intelligent Molecular Searcher from Logic Computing Network Based on Eu(III) Functionalized UMOFs for Environmental Monitoring. *Adv. Funct. Mater.* **2017**, *27*, 1700247. [[CrossRef](#)]

28. Xia, T.; Cui, Y.; Yang, Y.; Qian, G. Highly Stable Mixed-Lanthanide Metal–Organic Frameworks for Self-Referencing and Colorimetric Luminescent pH Sensing. *ChemNanoMat* **2017**, *3*, 51–57. [[CrossRef](#)]
29. Zhang, S.-Y.; Shi, W.; Cheng, P.; Zaworotko, M.J. A Mixed-Crystal Lanthanide Zeolite-like Metal–Organic Framework as a Fluorescent Indicator for Lysophosphatidic Acid, a Cancer Biomarker. *J. Am. Chem. Soc.* **2015**, *137*, 12203–12206. [[CrossRef](#)] [[PubMed](#)]
30. Hao, J.-N.; Yan, B. Determination of Urinary 1-Hydroxypyrene for Biomonitoring of Human Exposure to Polycyclic Aromatic Hydrocarbons Carcinogens by a Lanthanide-functionalized Metal-Organic Framework Sensor. *Adv. Funct. Mater.* **2017**, *27*, 1603856. [[CrossRef](#)]
31. Wu, S.; Lin, Y.; Liu, J.; Shi, W.; Yang, G.; Cheng, P. Rapid Detection of the Biomarkers for Carcinoid Tumors by a Water Stable Luminescent Lanthanide Metal–Organic Framework Sensor. *Adv. Funct. Mater.* **2018**, *28*, 1707169. [[CrossRef](#)]
32. Li, B.; Wen, H.-M.; Cui, Y.; Qian, G.; Chen, B. Multifunctional lanthanide coordination polymers. *Prog. Polym. Sci.* **2015**, *48*, 40–84. [[CrossRef](#)]
33. Xia, T.; Song, T.; Cui, Y.; Yang, Y.; Qian, G. A dye encapsulated terbium-based metal-organic framework for ratiometric temperature sensing. *Dalton Trans.* **2016**, *45*, 18689–18695. [[CrossRef](#)] [[PubMed](#)]
34. Lustig, W.P.; Mukherjee, S.; Rudd, N.D.; Desai, A.V.; Li, J.; Ghosh, S.K. Metal–organic frameworks: Functional luminescent and photonic materials for sensing applications. *Chem. Soc. Rev.* **2017**, *46*, 3242–3285. [[CrossRef](#)] [[PubMed](#)]
35. Yan, B. Lanthanide-Functionalized Metal–Organic Framework Hybrid Systems To Create Multiple Luminescent Centers for Chemical Sensing. *Acc. Chem. Res.* **2017**, *50*, 2789–2798. [[CrossRef](#)] [[PubMed](#)]
36. Cui, Y.; Li, B.; He, H.; Zhou, W.; Chen, B.; Qian, G. Metal–Organic Frameworks as Platforms for Functional Materials. *Acc. Chem. Res.* **2016**, *49*, 483–493. [[CrossRef](#)] [[PubMed](#)]
37. Kreno, L.E.; Leong, K.; Farha, O.K.; Allendorf, M.; Van Duyne, R.P.; Hupp, J.T. Metal-organic framework materials as chemical sensors. *Chem. Rev.* **2012**, *112*, 1105–1125. [[CrossRef](#)] [[PubMed](#)]
38. Zhang, Y.; Yuan, S.; Day, G.; Wang, X.; Yang, X.; Zhou, H.-C. Luminescent sensors based on metal–organic frameworks. *Coord. Chem. Rev.* **2017**, *354*, 28–45. [[CrossRef](#)]
39. Zacher, D.; Shekhah, O.; Wöll, C.; Fischer, R.A. Thin films of metal–organic frameworks. *Chem. Soc. Rev.* **2009**, *38*, 1418–1429. [[CrossRef](#)] [[PubMed](#)]
40. Yao, J.; Wang, H. Zeolitic imidazolate framework composite membranes and thin films: Synthesis and applications. *Chem. Soc. Rev.* **2014**, *43*, 4470–4493. [[CrossRef](#)] [[PubMed](#)]
41. Liu, J.; Woll, C. Surface-supported metal-organic framework thin films: Fabrication methods, applications, and challenges. *Chem. Soc. Rev.* **2017**, *46*, 5730–5770. [[CrossRef](#)] [[PubMed](#)]
42. Falcaro, P.; Ricco, R.; Doherty, C.M.; Liang, K.; Hill, A.J.; Styles, M.J. MOF positioning technology and device fabrication. *Chem. Soc. Rev.* **2014**, *43*, 5513–5560. [[CrossRef](#)] [[PubMed](#)]
43. Shekhah, O.; Liu, J.; Fischer, R.A.; Woll, C. MOF thin films: Existing and future applications. *Chem. Soc. Rev.* **2011**, *40*, 1081–1106. [[CrossRef](#)] [[PubMed](#)]
44. Bradshaw, D.; Garai, A.; Huo, J. Metal-organic framework growth at functional interfaces: Thin films and composites for diverse applications. *Chem. Soc. Rev.* **2012**, *41*, 2344–2381. [[CrossRef](#)] [[PubMed](#)]
45. Qiu, S.; Xue, M.; Zhu, G. Metal-organic framework membranes: From synthesis to separation application. *Chem. Soc. Rev.* **2014**, *43*, 6116–6140. [[CrossRef](#)] [[PubMed](#)]
46. Zhuang, J.-L.; Terfort, A.; Wöll, C. Formation of oriented and patterned films of metal–organic frameworks by liquid phase epitaxy: A review. *Coord. Chem. Rev.* **2016**, *307*, 391–424. [[CrossRef](#)]
47. Liu, Y.; Ng, Z.; Khan, E.A.; Jeong, H.-K.; Ching, C.-B.; Lai, Z. Synthesis of continuous MOF-5 membranes on porous α -alumina substrates. *Micropor. Mesopor. Mater.* **2009**, *118*, 296–301. [[CrossRef](#)]
48. Zacher, D.; Baunemann, A.; Hermes, S.; Fischer, R.A. Deposition of microcrystalline $[\text{Cu}_3(\text{btc})_2]$ and $[\text{Zn}_2(\text{bdc})_2(\text{dabco})]$ at alumina and silica surfaces modified with patterned self assembled organic monolayers: Evidence of surface selective and oriented growth. *J. Mater. Chem.* **2007**, *17*, 2785–2792. [[CrossRef](#)]
49. Shah, M.; Kwon, H.T.; Tran, V.; Sachdeva, S.; Jeong, H.-K. One step in situ synthesis of supported zeolitic imidazolate framework ZIF-8 membranes: Role of sodium formate. *Micropor. Mesopor. Mater.* **2013**, *165*, 63–69. [[CrossRef](#)]

50. Bux, H.; Chmelik, C.; van Baten, J.M.; Krishna, R.; Caro, J. Novel MOF-membrane for molecular sieving predicted by IR-diffusion studies and molecular modeling. *Adv. Mater.* **2010**, *22*, 4741–4743. [[CrossRef](#)] [[PubMed](#)]
51. Eslava, S.; Zhang, L.; Esconjauregui, S.; Yang, J.; Vanstreels, K.; Baklanov, M.R.; Saiz, E. Metal-organic framework ZIF-8 films as low- κ dielectrics in microelectronics. *Chem. Mater.* **2012**, *25*, 27–33. [[CrossRef](#)]
52. Guo, H.; Zhu, G.; Hewitt, I.J.; Qiu, S. “Twin copper source” growth of metal-organic framework membrane: $\text{Cu}_3(\text{BTC})_2$ with high permeability and selectivity for recycling H_2 . *J. Am. Chem. Soc.* **2009**, *131*, 1646–1647. [[CrossRef](#)] [[PubMed](#)]
53. Zou, X.; Zhu, G.; Hewitt, I.J.; Sun, F.; Qiu, S. Synthesis of a metal-organic framework film by direct conversion technique for VOCs sensing. *Dalton Trans.* **2009**, 3009–3013. [[CrossRef](#)] [[PubMed](#)]
54. Kayaert, S.; Bajpe, S.; Masschaele, K.; Breynaert, E.; Kirschhock, C.E.; Martens, J.A. Direct growth of Keggin polyoxometalates incorporated copper 1,3,5-benzenetricarboxylate metal organic framework films on a copper metal substrate. *Thin Solid Films* **2011**, *519*, 5437–5440. [[CrossRef](#)]
55. Kang, Z.; Xue, M.; Fan, L.; Ding, J.; Guo, L.; Gao, L.; Qiu, S. “Single nickel source” in situ fabrication of a stable homochiral MOF membrane with chiral resolution properties. *Chem. Commun.* **2013**, *49*, 10569–10571. [[CrossRef](#)] [[PubMed](#)]
56. Huang, A.; Dou, W.; Caro, J. Steam-stable zeolitic imidazolate framework ZIF-90 membrane with hydrogen selectivity through covalent functionalization. *J. Am. Chem. Soc.* **2010**, *132*, 15562–15564. [[CrossRef](#)] [[PubMed](#)]
57. Huang, A.; Bux, H.; Steinbach, F.; Caro, J. Molecular-sieve membrane with hydrogen permselectivity: ZIF-22 in LTA topology prepared with 3-aminopropyltriethoxysilane as covalent linker. *Angew. Chem. Int. Ed.* **2010**, *49*, 4958–4961. [[CrossRef](#)] [[PubMed](#)]
58. Arnold, M.; Kortunov, P.; Jones, D.J.; Nedellec, Y.; Kärger, J.; Caro, J. Oriented crystallisation on supports and anisotropic mass transport of the metal-organic framework manganese formate. *Eur. J. Inorg. Chem.* **2007**, *2007*, 60–64. [[CrossRef](#)]
59. Cao, F.; Zhang, C.; Xiao, Y.; Huang, H.; Zhang, W.; Liu, D.; Zhong, C.; Yang, Q.; Yang, Z.; Lu, X. Helium recovery by a Cu-BTC metal-organic-framework membrane. *Ind. Eng. Chem. Res.* **2012**, *51*, 11274–11278. [[CrossRef](#)]
60. So, M.C.; Jin, S.; Son, H.J.; Wiederrecht, G.P.; Farha, O.K.; Hupp, J.T. Layer-by-layer fabrication of oriented porous thin films based on porphyrin-containing metal-organic frameworks. *J. Am. Chem. Soc.* **2013**, *135*, 15698–15701. [[CrossRef](#)] [[PubMed](#)]
61. Betard, A.; Fischer, R.A. Metal-organic framework thin films: From fundamentals to applications. *Chem. Rev.* **2012**, *112*, 1055–1083. [[CrossRef](#)] [[PubMed](#)]
62. Zhang, J.; Xia, T.; Zhao, D.; Cui, Y.; Yang, Y.; Qian, G. In situ secondary growth of Eu(III)-organic framework film for fluorescence sensing of sulfur dioxide. *Sensor. Actuat. B-Chem.* **2018**, *260*, 63–69. [[CrossRef](#)]
63. Yusenkov, K.; Meilikhov, M.; Zacher, D.; Wieland, F.; Sternemann, C.; Stammer, X.; Ladnorg, T.; Wöll, C.; Fischer, R.A. Step-by-step growth of highly oriented and continuous seeding layers of $[\text{Cu}_2(\text{ndc})_2(\text{dabco})]$ on bare oxide and nitride substrates. *CrystEngComm* **2010**, *12*, 2086–2090. [[CrossRef](#)]
64. Yoo, Y.; Jeong, H.-K. Heteroepitaxial Growth of Isorecticular Metal-Organic Frameworks and Their Hybrid Films. *Cryst. Growth Des.* **2010**, *10*, 1283–1288. [[CrossRef](#)]
65. Falcaro, P.; Okada, K.; Hara, T.; Ikigaki, K.; Tokudome, Y.; Thornton, A.W.; Hill, A.J.; Williams, T.; Doonan, C.; Takahashi, M. Centimetre-scale micropore alignment in oriented polycrystalline metal-organic framework films via heteroepitaxial growth. *Nat. Mater.* **2017**, *16*, 342–348. [[CrossRef](#)] [[PubMed](#)]
66. Mueller, U.; Puetter, H.; Hesse, M.; Schubert, M.; Wessel, H.; Huff, J.; Guzman, M. Method for Electrochemical Production of a Crystalline Porous Metal Organic Skeleton Material. U.S. Patent 7,968,739B2, 28 June 2011.
67. Li, W.-J.; Tu, M.; Cao, R.; Fischer, R.A. Metal-organic framework thin films: Electrochemical fabrication techniques and corresponding applications & perspectives. *J. Mater. Chem. A* **2016**, *4*, 12356–12369.
68. Alizadeh, S.; Nematollahi, D. Electrochemically Assisted Self-Assembly Technique for the Fabrication of Mesoporous Metal-Organic Framework Thin Films: Composition of 3D Hexagonally Packed Crystals with 2D Honeycomb-like Mesopores. *J. Am. Chem. Soc.* **2017**, *139*, 4753–4761. [[CrossRef](#)] [[PubMed](#)]
69. Ameloot, R.; Stappers, L.; Franssaer, J.; Alaerts, L.; Sels, B.F.; De Vos, D.E. Patterned growth of metal-organic framework coatings by electrochemical synthesis. *Chem. Mater.* **2009**, *21*, 2580–2582. [[CrossRef](#)]

70. Li, W.-J.; Lü, J.; Gao, S.-Y.; Li, Q.-H.; Cao, R. Electrochemical preparation of metal–organic framework films for fast detection of nitro explosives. *J. Mater. Chem. A* **2014**, *2*, 19473–19478. [[CrossRef](#)]
71. Campagnol, N.; Van Assche, T.; Boudewijns, T.; Denayer, J.; Binnemans, K.; De Vos, D.; Fransaer, J. High pressure, high temperature electrochemical synthesis of metal–organic frameworks: Films of MIL-100(Fe) and HKUST-1 in different morphologies. *J. Mater. Chem. A* **2013**, *1*, 5827–5830. [[CrossRef](#)]
72. Li, W.-J.; Liu, J.; Sun, Z.-H.; Liu, T.-F.; Lü, J.; Gao, S.-Y.; He, C.; Cao, R.; Luo, J.-H. Integration of metal–organic frameworks into an electrochemical dielectric thin film for electronic applications. *Nat. Commun.* **2016**, *7*, 11830. [[CrossRef](#)] [[PubMed](#)]
73. Hod, I.; Bury, W.; Karlin, D.M.; Deria, P.; Kung, C.W.; Katz, M.J.; So, M.; Klahr, B.; Jin, D.; Chung, Y.W. Directed growth of electroactive metal-organic framework thin films using electrophoretic deposition. *Adv. Mater.* **2014**, *26*, 6295–6300. [[CrossRef](#)] [[PubMed](#)]
74. Feng, J.F.; Gao, S.Y.; Shi, J.; Liu, T.F.; Cao, R. C-QDs@UiO-66-(COOH)₂ Composite Film via Electrophoretic Deposition for Temperature Sensing. *Inorg. Chem.* **2018**, *57*, 2447–2454. [[CrossRef](#)] [[PubMed](#)]
75. Feng, J.F.; Gao, S.Y.; Liu, T.F.; Shi, J.; Cao, R. Preparation of Dual-Emitting Ln@UiO-66-Hybrid Films via Electrophoretic Deposition for Ratiometric Temperature Sensing. *ACS Appl. Mater. Interfaces* **2018**, *10*, 6014–6023. [[CrossRef](#)] [[PubMed](#)]
76. Li, M.; Dincă, M. Selective formation of biphasic thin films of metal–organic frameworks by potential-controlled cathodic electrodeposition. *Chem. Sci.* **2014**, *5*, 107–111. [[CrossRef](#)]
77. Liu, H.; Wang, H.; Chu, T.; Yu, M.; Yang, Y. An electrodeposited lanthanide MOF thin film as a luminescent sensor for carbonate detection in aqueous solution. *J. Mater. Chem. C* **2014**, *2*, 8683–8690. [[CrossRef](#)]
78. Chernikova, V.; Shekhah, O.; Eddaoudi, M. Advanced Fabrication Method for the Preparation of MOF Thin Films: Liquid-Phase Epitaxy Approach Meets Spin Coating Method. *ACS Appl. Mater. Interfaces* **2016**, *8*, 20459–20464. [[CrossRef](#)] [[PubMed](#)]
79. Guo, H.; Zhu, Y.; Qiu, S.; Lercher, J.A.; Zhang, H. Coordination Modulation Induced Synthesis of Nanoscale Eu_{1-x}Tb_x-Metal–Organic Frameworks for Luminescent Thin Films. *Adv. Mater.* **2010**, *22*, 4190–4192. [[CrossRef](#)] [[PubMed](#)]
80. Demessence, A.; Horcajada, P.; Serre, C.; Boissiere, C.; Grosso, D.; Sanchez, C.; Ferey, G. Elaboration and properties of hierarchically structured optical thin films of MIL-101(Cr). *Chem. Commun.* **2009**, 7149–7151. [[CrossRef](#)] [[PubMed](#)]
81. Jiang, D.; Burrows, A.D.; Xiong, Y.; Edler, K.J. Facile synthesis of crack-free metal–organic framework films on alumina by a dip-coating route in the presence of polyethylenimine. *J. Mater. Chem. A* **2013**, *1*, 5497–5500. [[CrossRef](#)]
82. Yehia, H.; Pisklak, T.; Ferraris, J.; Balkus, K.; Musselman, I. Methane facilitated transport using copper(II) biphenyl dicarboxylate-triethylenediamine/poly (3-acetoxyethylthiophene) mixed matrix membranes. *Abstr. Pap. Am. Chem. Soc.* **2004**, *227*, U351.
83. Campbell, J.; Székely, G.; Davies, R.P.; Braddock, D.C.; Livingston, A.G. Fabrication of hybrid polymer/metal organic framework membranes: Mixed matrix membranes versus in situ growth. *J. Mater. Chem. A* **2014**, *2*, 9260–9271. [[CrossRef](#)]
84. Zornoza, B.; Tellez, C.; Coronas, J.; Gascon, J.; Kapteijn, F. Metal-organic framework based mixed matrix membranes: An increasingly important field of research with a large application potential. *Micropor. Mesopor. Mater.* **2013**, *166*, 67–78. [[CrossRef](#)]
85. Liu, X.; Wang, C.; Wang, B.; Li, K. Novel Organic-Dehydration Membranes Prepared from Zirconium Metal–Organic Frameworks. *Adv. Funct. Mater.* **2017**, *27*, 1604311. [[CrossRef](#)]
86. Seoane, B.; Coronas, J.; Gascon, I.; Etxebarria Benavides, M.; Karvan, O.; Caro, J.; Kapteijn, F.; Gascon, J. Metal-organic framework based mixed matrix membranes: A solution for highly efficient CO₂ capture? *Chem. Soc. Rev.* **2015**, *44*, 2421–2454. [[CrossRef](#)] [[PubMed](#)]
87. Denny, M.S., Jr.; Cohen, S.M. In Situ Modification of Metal–Organic Frameworks in Mixed-Matrix Membranes. *Angew. Chem. Int. Ed.* **2015**, *54*, 9029–9032. [[CrossRef](#)] [[PubMed](#)]
88. Cui, Y.; Yue, Y.; Qian, G.; Chen, B. Luminescent functional metal–organic frameworks. *Chem. Rev.* **2012**, *112*, 1126–1162. [[CrossRef](#)] [[PubMed](#)]
89. Cui, Y.; Chen, B.; Qian, G. Lanthanide metal–organic frameworks for luminescent sensing and light-emitting applications. *Coord. Chem. Rev.* **2014**, *273*, 76–86. [[CrossRef](#)]

90. Zhang, F.; Zhang, G.; Yao, H.; Wang, Y.; Chu, T.; Yang, Y. A europium(III) based nano-flake MOF film for efficient fluorescent sensing of picric acid. *Microchim. Acta* **2017**, *184*, 1207–1213. [[CrossRef](#)]
91. Wang, Z.; Liu, H.; Wang, S.; Rao, Z.; Yang, Y. A luminescent Terbium-Succinate MOF thin film fabricated by electrodeposition for sensing of Cu^{2+} in aqueous environment. *Sens. Actuators B-Chem.* **2015**, *220*, 779–787. [[CrossRef](#)]
92. Gao, Y.; Yu, G.; Liu, K.; Wang, B. Luminescent mixed-crystal Ln-MOF thin film for the recognition and detection of pharmaceuticals. *Sens. Actuators B-Chem.* **2018**, *257*, 931–935. [[CrossRef](#)]
93. Liu, H.; Chu, T.; Rao, Z.; Wang, S.; Yang, Y.; Wong, W.-T. The Tunable White-Light and Multicolor Emission in An Electrodeposited Thin Film of Mixed Lanthanide Coordination Polymers. *Adv. Opt. Mater.* **2015**, *3*, 1545–1550. [[CrossRef](#)]
94. Dou, Z.; Yu, J.; Cui, Y.; Yang, Y.; Wang, Z.; Yang, D.; Qian, G. Luminescent Metal–Organic Framework Films As Highly Sensitive and Fast-Response Oxygen Sensors. *J. Am. Chem. Soc.* **2014**, *136*, 5527–5530. [[CrossRef](#)] [[PubMed](#)]
95. Zhang, J.; Yue, D.; Xia, T.; Cui, Y.; Yang, Y.; Qian, G. A luminescent metal-organic framework film fabricated on porous Al_2O_3 substrate for sensitive detecting ammonia. *Micropor. Mesopor. Mater.* **2017**, *253*, 146–150. [[CrossRef](#)]
96. Streit, H.C.; Adlung, M.; Shekhah, O.; Stammer, X.; Arslan, H.K.; Zybalyo, O.; Ladnorg, T.; Gliemann, H.; Franzreb, M.; Woll, C.; et al. Surface-anchored MOF-based photonic antennae. *ChemPhysChem* **2012**, *13*, 2699–2702. [[CrossRef](#)] [[PubMed](#)]
97. Cui, Y.; Xu, H.; Yue, Y.; Guo, Z.; Yu, J.; Chen, Z.; Gao, J.; Yang, Y.; Qian, G.; Chen, B. A Luminescent Mixed-Lanthanide Metal–Organic Framework Thermometer. *J. Am. Chem. Soc.* **2012**, *134*, 3979–3982. [[CrossRef](#)] [[PubMed](#)]
98. Cadiou, A.; Brites, C.D.S.; Costa, P.M.F.J.; Ferreira, R.A.S.; Rocha, J.; Carlos, L.D. Ratiometric Nanothermometer Based on an Emissive Ln^{3+} -Organic Framework. *ACS Nano* **2013**, *7*, 7213–7218. [[CrossRef](#)] [[PubMed](#)]
99. Xia, T.; Cui, Y.; Yang, Y.; Qian, G. A luminescent ratiometric thermometer based on thermally coupled levels of a Dy-MOF. *J. Mater. Chem. C* **2017**, *5*, 5044–5047. [[CrossRef](#)]
100. Shen, X.; Yan, B. Polymer hybrid thin films based on rare earth ion-functionalized MOF: Photoluminescence tuning and sensing as a thermometer. *Dalton Trans.* **2015**, *44*, 1875–1881. [[CrossRef](#)] [[PubMed](#)]
101. Liu, X.; Fu, W.; Bouwman, E. One-step growth of lanthanoid metal-organic framework (MOF) films under solvothermal conditions for temperature sensing. *Chem. Commun.* **2016**, *52*, 6926–6929. [[CrossRef](#)] [[PubMed](#)]
102. Carter, K.P.; Young, A.M.; Palmer, A.E. Fluorescent sensors for measuring metal ions in living systems. *Chem. Rev.* **2014**, *114*, 4564–4601. [[CrossRef](#)] [[PubMed](#)]
103. Xiao, Y.; Cui, Y.; Zheng, Q.; Xiang, S.; Qian, G.; Chen, B. A microporous luminescent metal-organic framework for highly selective and sensitive sensing of Cu^{2+} in aqueous solution. *Chem. Commun.* **2010**, *46*, 5503–5505. [[CrossRef](#)] [[PubMed](#)]
104. Wang, X.; Qin, T.; Bao, S.-S.; Zhang, Y.-C.; Shen, X.; Zheng, L.-M.; Zhu, D. Facile synthesis of a water stable 3D Eu-MOF showing high proton conductivity and its application as a sensitive luminescent sensor for Cu^{2+} ions. *J. Mater. Chem. A* **2016**, *4*, 16484–16489. [[CrossRef](#)]
105. Cho, W.; Lee, H.J.; Choi, G.; Choi, S.; Oh, M. Dual Changes in Conformation and Optical Properties of Fluorophores within a Metal-Organic Framework during Framework Construction and Associated Sensing Event. *J. Am. Chem. Soc.* **2014**, *136*, 12201–12204. [[CrossRef](#)] [[PubMed](#)]
106. Wang, Y.; Chu, T.; Yu, M.; Liu, H.; Yang, Y. One step cathodically electrodeposited $[\text{Tb}_2(\text{BDC})_3(\text{H}_2\text{O})_4]_n$ thin film as a luminescent probe for Cu^{2+} detection. *RSC Adv.* **2014**, *4*, 58178–58183. [[CrossRef](#)]
107. Tan, H.; Liu, B.; Chen, Y. Lanthanide Coordination Polymer Nanoparticles for Sensing of Mercury(II) by Photoinduced Electron Transfer. *ACS Nano* **2012**, *6*, 10505–10511. [[CrossRef](#)] [[PubMed](#)]
108. Zhu, Y.M.; Zeng, C.H.; Chu, T.S.; Wang, H.M.; Yang, Y.Y.; Tong, Y.X.; Su, C.Y.; Wong, W.T. A novel highly luminescent LnMOF film: A convenient sensor for Hg^{2+} detecting. *J. Mater. Chem. A* **2013**, *1*, 11312–11319. [[CrossRef](#)]
109. Xia, T.; Song, T.; Zhang, G.; Cui, Y.; Yang, Y.; Wang, Z.; Qian, G. A Terbium Metal–Organic Framework for Highly Selective and Sensitive Luminescence Sensing of Hg^{2+} Ion in Aqueous Solution. *Chem. Eur. J.* **2016**, *22*, 18429–18434. [[CrossRef](#)] [[PubMed](#)]

110. Yang, J.; Wang, Z.; Li, Y.; Zhuang, Q.; Zhao, W.; Gu, J. Porphyrinic MOFs for reversible fluorescent and colorimetric sensing of mercury(II) ions in aqueous phase. *RSC Adv.* **2016**, *6*, 69807–69814. [[CrossRef](#)]
111. Wen, L.; Zheng, X.; Lv, K.; Wang, C.; Xu, X. Two Amino-Decorated Metal–Organic Frameworks for Highly Selective and Quantitatively Sensing of Hg(II) and Cr(VI) in Aqueous Solution. *Inorg. Chem.* **2015**, *54*, 7133–7135. [[CrossRef](#)] [[PubMed](#)]
112. Zhang, X.; Xia, T.; Jiang, K.; Cui, Y.; Yang, Y.; Qian, G. Highly sensitive and selective detection of mercury(II) based on a zirconium metal-organic framework in aqueous media. *J. Solid State Chem.* **2017**, *253*, 277–281. [[CrossRef](#)]
113. Rudd, N.D.; Wang, H.; Fuentes-Fernandez, E.M.; Teat, S.J.; Chen, F.; Hall, G.; Chabal, Y.J.; Li, J. Highly Efficient Luminescent Metal-Organic Framework for the Simultaneous Detection and Removal of Heavy Metals from Water. *ACS Appl. Mater. Interfaces* **2016**, *8*, 30294–30303. [[CrossRef](#)] [[PubMed](#)]
114. Yee, K.-K.; Reimer, N.; Liu, J.; Cheng, S.-Y.; Yiu, S.-M.; Weber, J.; Stock, N.; Xu, Z. Effective Mercury Sorption by Thiol-Laced Metal–Organic Frameworks: In Strong Acid and the Vapor Phase. *J. Am. Chem. Soc.* **2013**, *135*, 7795–7798. [[CrossRef](#)] [[PubMed](#)]
115. Feng, J.F.; Yang, X.; Gao, S.Y.; Shi, J.; Cao, R. Facile and Rapid Growth of Nanostructured Ln-BTC Metal-Organic Framework Films by Electrophoretic Deposition for Explosives sensing in Gas and Cr³⁺ Detection in Solution. *Langmuir* **2017**, *33*, 14238–14243. [[CrossRef](#)] [[PubMed](#)]
116. Jia, X.X.; Yao, R.X.; Zhang, F.Q.; Zhang, X.M. A Fluorescent Anionic MOF with Zn₄(trz)₂ Chain for Highly Selective Visual Sensing of Contaminants: Cr(III) Ion and TNP. *Inorg. Chem.* **2017**, *56*, 2690–2696. [[CrossRef](#)] [[PubMed](#)]
117. Sun, N.-N.; Yan, B. Rapid and facile ratiometric detection of CO₃²⁻ based on heterobimetallic metal–organic frameworks (Eu/Pt-MOFs). *Dyes Pigments* **2017**, *142*, 1–7. [[CrossRef](#)]
118. Lian, X.; Yan, B. A postsynthetically modified MOF hybrid as a ratiometric fluorescent sensor for anion recognition and detection. *Dalton Trans.* **2016**, *45*, 18668–18675. [[CrossRef](#)] [[PubMed](#)]
119. Dou, Z.; Cai, J.; Cui, Y.; Yu, J.; Xia, T.; Yang, Y.; Qian, G. Preparation and Gas Separation Properties of Metal-Organic Framework Membranes. *Z. Anorg. Allg. Chem.* **2015**, *641*, 792–796. [[CrossRef](#)]
120. Xu, R.; Wang, Y.; Duan, X.; Lu, K.; Micheroni, D.; Hu, A.; Lin, W. Nanoscale Metal–Organic Frameworks for Ratiometric Oxygen Sensing in Live Cells. *J. Am. Chem. Soc.* **2016**, *138*, 2158–2161. [[CrossRef](#)] [[PubMed](#)]
121. Zhang, F.; Wang, Y.; Chu, T.; Wang, Z.; Li, W.; Yang, Y. A facile fabrication of electrodeposited luminescent MOF thin films for selective and recyclable sensing of nitroaromatic explosives. *Analyst* **2016**, *141*, 4502–4510. [[CrossRef](#)] [[PubMed](#)]
122. Zhao, C.W.; Ma, J.P.; Liu, Q.K.; Wang, X.R.; Liu, Y.; Yang, J.; Yang, J.S.; Dong, Y.B. An in situ self-assembled Cu₄I₄-MOF-based mixed matrix membrane: A highly sensitive and selective naked-eye sensor for gaseous HCl. *Chem. Commun.* **2016**, *52*, 5238–5241. [[CrossRef](#)] [[PubMed](#)]
123. Wang, Y.; Zhang, G.; Zhang, F.; Chu, T.; Yang, Y. A novel lanthanide MOF thin film: The highly performance self-calibrating luminescent sensor for detecting formaldehyde as an illegal preservative in aquatic product. *Sens. Actuators B-Chem.* **2017**, *251*, 667–673. [[CrossRef](#)]
124. Zhang, F.; Yao, H.; Chu, T.; Zhang, G.; Wang, Y.; Yang, Y. A Lanthanide MOF Thin-Film Fixed with Co₃O₄ Nano-Anchors as a Highly Efficient Luminescent Sensor for Nitrofurant Antibiotics. *Chem. Eur. J.* **2017**, *23*, 10293–10300. [[CrossRef](#)] [[PubMed](#)]
125. Zhang, F.; Yao, H.; Zhao, Y.; Li, X.; Zhang, G.; Yang, Y. Mixed matrix membranes incorporated with Ln-MOF for selective and sensitive detection of nitrofurant antibiotics based on inner filter effect. *Talanta* **2017**, *174*, 660–666. [[CrossRef](#)] [[PubMed](#)]

